Tregs restrain dendritic cell autophagy to ameliorate autoimmunity

Themis Alissafi, … , Ken Cadwell, Panayotis Verginis

Research Article   Autoimmunity   Immunology

Design of efficacious Treg-based therapies and establishment of clinical tolerance in autoimmune diseases have proven to be challenging. The clinical implementation of Treg immunotherapy has been hampered by various impediments related to the stability and isolation procedures of Tregs as well as the specific in vivo targets of Treg modalities. Herein, we have demonstrated that Foxp3$^+$ Tregs potently suppress autoimmune responses in vivo through inhibition of the autophagic machinery in DCs in a cytotoxic T-lymphocyte–associated protein 4–dependent (CTLA4-dependent) manner. Autophagy-deficient DCs exhibited reduced immunogenic potential and failed to prime autoantigen-specific CD4$^+$ T cells to mediate autoimmunity. Mechanistically, CTLA4 binding promoted activation of the PI3K/Akt/mTOR axis and FoxO1 nuclear exclusion in DCs, leading to decreased transcription of the autophagy component microtubule-associated protein 1 light chain 3β (*Lc3b*). Human DCs treated with CTLA4-Ig, a fusion protein composed of the Fc region of IgG1 and the extracellular domain of CTLA4 (also known as abatacept, marketed as Orencia), demonstrated reduced levels of autophagosome formation, while DCs from CTLA4-Ig–treated rheumatoid arthritis patients displayed diminished *LC3B* transcripts. Collectively, our data identify the canonical autophagy pathway in DCs as a molecular target of Foxp3$^+$ Treg–mediated suppression that leads to amelioration of autoimmune responses. These findings may pave the way for the development of therapeutic protocols that exploit Tregs for the treatment of autoimmunity as well as diseases [...]

Find the latest version:

https://jci.me/92079/pdf

Tregs restrain dendritic cell autophagy to ameliorate autoimmunity

Themis Alissafi,[1] Aggelos Banos,[1] Louis Boon,[2] Tim Sparwasser,[3] Alessandra Ghigo,[4] Kajsa Wing,[5] Dimitrios Vassilopoulos,[6] Dimitrios Boumpas,[1,7] Triantafyllos Chavakis,[8] Ken Cadwell,[9,10] and Panayotis Verginis[1]

[1]Biomedical Research Foundation of the Academy of Athens, Athens, Greece. [2]Bioceros BV, Utrecht, Netherlands. [3]Institute of Infection Immunology, TWINCORE, Centre for Experimental and Clinical Infection Research, Hannover, Germany. [4]Molecular Biotechnology Center, Department of Molecular Biotechnology and Health Sciences, University of Torino, Torino, Italy. [5]Division of Medical Inflammation Research, Department of Medical Biochemistry and Biophysics, Karolinska Institutet, Stockholm, Sweden. [6]Joint Rheumatology Program, Clinical Immunology-Rheumatology Unit, National and Kapodistrian University of Athens Medical School, Hippokration General Hospital, Athens, Greece. [7]Joint Rheumatology Program, 4th Department of Medicine, Attikon University Hospital, National and Kapodistrian University of Athens Medical School, Athens, Greece. [8]Department of Clinical Pathobiochemistry, Institute for Clinical Chemistry and Laboratory Medicine and Department of Internal Medicine, University of Dresden, Dresden, Germany. [9]Kimmel Center for Biology and Medicine at the Skirball Institute, New York, New York, USA. [10]Departments of Microbiology and Medicine, New York University School of Medicine, New York, New York, USA.

Design of efficacious Treg-based therapies and establishment of clinical tolerance in autoimmune diseases have proven to be challenging. The clinical implementation of Treg immunotherapy has been hampered by various impediments related to the stability and isolation procedures of Tregs as well as the specific in vivo targets of Treg modalities. Herein, we have demonstrated that Foxp3+ Tregs potently suppress autoimmune responses in vivo through inhibition of the autophagic machinery in DCs in a cytotoxic T-lymphocyte–associated protein 4–dependent (CTLA4-dependent) manner. Autophagy-deficient DCs exhibited reduced immunogenic potential and failed to prime autoantigen-specific CD4+ T cells to mediate autoimmunity. Mechanistically, CTLA4 binding promoted activation of the PI3K/Akt/mTOR axis and FoxO1 nuclear exclusion in DCs, leading to decreased transcription of the autophagy component microtubule-associated protein 1 light chain 3β (*Lc*3b). Human DCs treated with CTLA4-Ig, a fusion protein composed of the Fc region of IgG1 and the extracellular domain of CTLA4 (also known as abatacept, marketed as Orencia), demonstrated reduced levels of autophagosome formation, while DCs from CTLA4-Ig–treated rheumatoid arthritis patients displayed diminished *LC3B* transcripts. Collectively, our data identify the canonical autophagy pathway in DCs as a molecular target of Foxp3+ Treg–mediated suppression that leads to amelioration of autoimmune responses. These findings may pave the way for the development of therapeutic protocols that exploit Tregs for the treatment of autoimmunity as well as diseases in which disturbed tolerance is a common denominator.

Introduction

Autoimmune diseases develop upon aberrant activation of lymphocytes mainly due to failure of self-tolerance. Although current therapeutic regimens have replaced the generalized immunosuppressive strategies in the treatment of autoimmune diseases, a substantial proportion of patients fail to achieve clinical remission and to reestablish tolerance. Foxp3+ Tregs are essential for immune homeostasis, and their absence leads to fatal systemic autoimmunity in mice and humans (1, 2). This pivotal role of Tregs has generated an impetus for exploiting them as therapeutic targets in autoimmune diseases. Despite the growing body of knowledge of Treg biology, major caveats still have hindered the development of Treg-based therapies. Importantly, the cellular targets and the molecular mechanisms of Foxp3+ Treg–mediated suppression in vivo are poorly understood.

DCs are a prominent target for Foxp3+ Treg–mediated suppression during the early phases of an immune response. Treg-suppressive activity is abrogated upon inhibition of Treg-DC contact in vitro (3), and intravital microscopy studies elegantly demonstrated a Treg-DC interaction in vivo (4–6), strengthening the notion for a DC contact–dependent Treg–mediated suppression. Among the different molecules that have been implicated in Treg-mediated suppression (2), cytoxic T-lymphocyte–associated protein 4 (CTLA4) has received considerable attention, since it is constitutively expressed by Tregs, while conditional ablation of *Ctla4* expression on Tregs results in a scurfy-like phenotype in mice that develop a lymphoproliferative disease (7, 8). CTLA4 binds to B7.1/B7.2 molecules on DCs, delivering negative costimulatory signals that inhibit their immunogenic potential either through induction of transendocytosis of B7 molecules (9) or via induction of indoleamine-pyrrole 2,3-dioxygenase (IDO) enzyme, suggesting CTLA4-mediated reverse signaling in DCs (10, 11); however, this notion has been challenged by other reports (12). Therefore, the precise molecular pathways implicated in CTLA4-dependent inhibition of DC function by Tregs remain elusive.

Autophagy is a fundamental lysosomal catabolic pathway involving degradation of cytosolic proteins and organelles to maintain cell homeostasis. Emerging data have demonstrated an essential role of autophagy during innate and adaptive immune responses (8, 13, 14). Thymic generation, peripheral survival, and function of T lymphocytes are influenced by the levels of autophagy (14–16). Furthermore, induction of autophagy facilitates the delivery of antigenic peptides to the MHC class II–loading compartment and subsequent presentation to CD4$^+$ T cells (17–21). Whether autophagy constitutes a target of Foxp3$^+$ Treg–mediated suppression and induction of tolerance is unknown.

Herein, we demonstrate that Foxp3$^+$ Tregs impair the autophagic machinery of DCs in a CTLA4-dependent manner. Autophagy-deficient DCs showed diminished immunogenic potential and failed to prime autoantigen-specific CD4$^+$ T cells in vivo. Importantly, CTLA4 binding enhanced activation of the PI3K/Akt/mTOR pathway and induced the translocation of FoxO1 from the nucleus, a process that downregulated the transcription of microtubule-associated protein 1 light chain 3β (*Lc3b*) and the formation of autophagosomes. Finally, treatment of human DCs with a fusion protein composed of the Fc region of IgG1 and the extracellular domain of CTLA4 (CTLA4-Ig, also known as abatacept; marketed as Orencia), an approved biologic therapy for rheumatoid arthritis (RA), demonstrated reduced levels of autophagosome formation and mediated nuclear exclusion of FoxO1. Collectively, our results delineate a molecular mechanism of Foxp3$^+$ Treg–mediated suppression of DC function via CTLA4-dependent downregulation of autophagy that results in inhibition of autoimmune responses.

Results

Foxp3$^+$ Tregs inhibit autophagolysosome formation in DCs. To gain insights into the molecular targets underlying the Treg-mediated modulation of DC function, we focused on the transcriptomic analysis of DCs, derived from a model of Foxp3$^+$ Treg–mediated induction of tolerance published by our group (22). Hierarchical clustering, using Genes@Work (23) with Pearson correlation and center of mass, pointed to an enrichment of genes encoding molecules involved in autophagy-related biological processes (Figure 1A). Emerging literature implicates autophagy as an essential mechanism in antigen loading to MHC II (17–19) and antigen presentation by DCs (20). To examine whether Foxp3$^+$ Tregs exert their function through modulation of autophagy in DCs, we determined the expression levels of autophagy related 16 like 1 (*Atg16l1*) and autophagy related 5 (*Atg5*) in isolated DCs from draining lymph nodes (dLNs) of MOG$_{35–55}$–infused/MOG$_{35–55}$–immunized (tolerized), and MOG$_{35–55}$–immunized (control) mice, where MOG indicates myelin oligodendrocyte glycoprotein. *Atg16l1* was among the most downregulated genes in DCs from tolerized mice, as indicated by the microarray data, and forms an E3-like ligase complex with ATG5-ATG12 that is required for the ligation of the LC3b homologue ATG8 (24, 25). Expression of both *Atg16l1* and *Atg5* genes was significantly downregulated in tolerized DCs compared with control DCs. Importantly, ablation of Foxp3$^+$ Tregs in tolerized DEREG mice (which express diphtheria toxin [DT] receptor under the control of the *Foxp3* promoter; treatment with DT results in tolerized/Foxp3$^+$ Treg–depleted mice) restored the expression of autophagy genes (Figure 1B).

Following the updated guidelines for the assessment of autophagy (26), we examined the expression of LC3II/LC3I in DC lysates, since increased expression of LC3II denotes enriched formation of autophagosomes (26, 27) as well as the degradation of sequestosome 1 (SQSTM1, also known as p62), an adaptor protein that targets ubiquitinated proteins for lysosomal degradation via the autophagy pathway (28, 29). Notably, the LC3II/LC3I ratio was decreased, whereas p62 levels were increased in DCs from tolerized mice compared with control and tolerized/Foxp3$^+$ Treg–depleted mice (Figure 1C). Using immunofluorescence microscopy, we assessed formation of functional autophagolysosomes based on the expression of LC3, the lysosomal-associated membrane protein 1 (LAMP-1), and p62. To this end, significantly reduced autophagolysosome formation and increased accumulation of p62 were demonstrated in DCs from tolerized mice, whereas autophagolysosome function was restored in control and tolerized/Foxp3$^+$ Treg–depleted mice (Figure 1D). Consistently, ex vivo–isolated DCs from nontolerized Foxp3$^+$ Treg–depleted MOG$_{35–55}$/CFA–immunized DEREG animals (Foxp3$^+$ Treg depleted) demonstrated increased autophagic activity and enhanced autophagolysosomal degradation (Supplemental Figure 1A; supplemental material available online with this article; https://doi.org/10.1172/JCI92079DS1). Collectively, these results suggest that Foxp3$^+$ Tregs modulate the operation of the autophagy pathway in DCs through inhibition of autophagolysosome formation.

Foxp3$^+$ Tregs impair DC autophagy via modulation of the PI3K/Akt/mTOR axis. To provide direct evidence for the Foxp3$^+$ Treg–mediated inhibition of autophagy in DCs, we cocultured highly pure naive antigen-specific CD4$^+$Va2$^+$CD25$^-$ (Tn) or CD4$^+$Va2$^+$CD25$^+$ (Tregs, >90% were Foxp3$^+$; data not shown) cells, isolated from ovalbumin-specific TCR-transgenic (OVA-TCR) mice (hereafter referred to as OT-II mice), with DCs from syngeneic LC3-GFP mice in the presence of OVA$_{323–339}$ peptide. As shown in Supplemental Figure 2A, Tregs inhibited LC3-GFP aggregates, a marker of autophagosome formation, in DCs as compared with Tn cells. Importantly, addition of Tregs to Tn-DC cocultures restrained autophagosome formation in DCs (Supplemental Figure 2A).

To obtain in vivo evidence for our hypothesis, we performed adoptive transfer of highly pure CD4$^+$Foxp3-GFP$^+$ and CD4$^+$Foxp3-GFP$^-$ cells into MOG$_{35–55}$–immunized recombination activating gene 1–deficient (*Rag1$^{-/-}$*) mice. Assessment of autophagy in DC cell lysates showed decreased levels of LC3II in Foxp3$^+$ Treg–transferred mice (hereafter referred as Foxp3$^+$/DCs) as compared with DCs isolated from mice injected with Foxp3-GFP$^-$ cells (hereafter referred as Foxp3$^-$/DCs) (Supplemental Figure 2B). In support, confocal fluorescence microscopy demonstrated significantly reduced induction of autophagy pathway and formation of functional autophagolysosomes in Foxp3$^+$ Treg–exposed DCs (Figure 2A). These findings reveal that Foxp3$^+$ Tregs directly regulate autophagy in DCs both in vitro and in vivo.

Next, we sought to determine the intracellular signaling events mediating the Foxp3$^+$ Treg–dependent downregulation of DC autophagy. The kinase mTOR-dependent pathway is the best-characterized regulator of autophagy, and activation of the PI3K/Akt axis is an upstream modulator of mTOR activity (30). To this end, DCs isolated from Foxp3$^+$ Treg–transferred *Rag1$^{-/-}$* mice exhibited elevated phosphorylation of mTOR, the p85 sub-
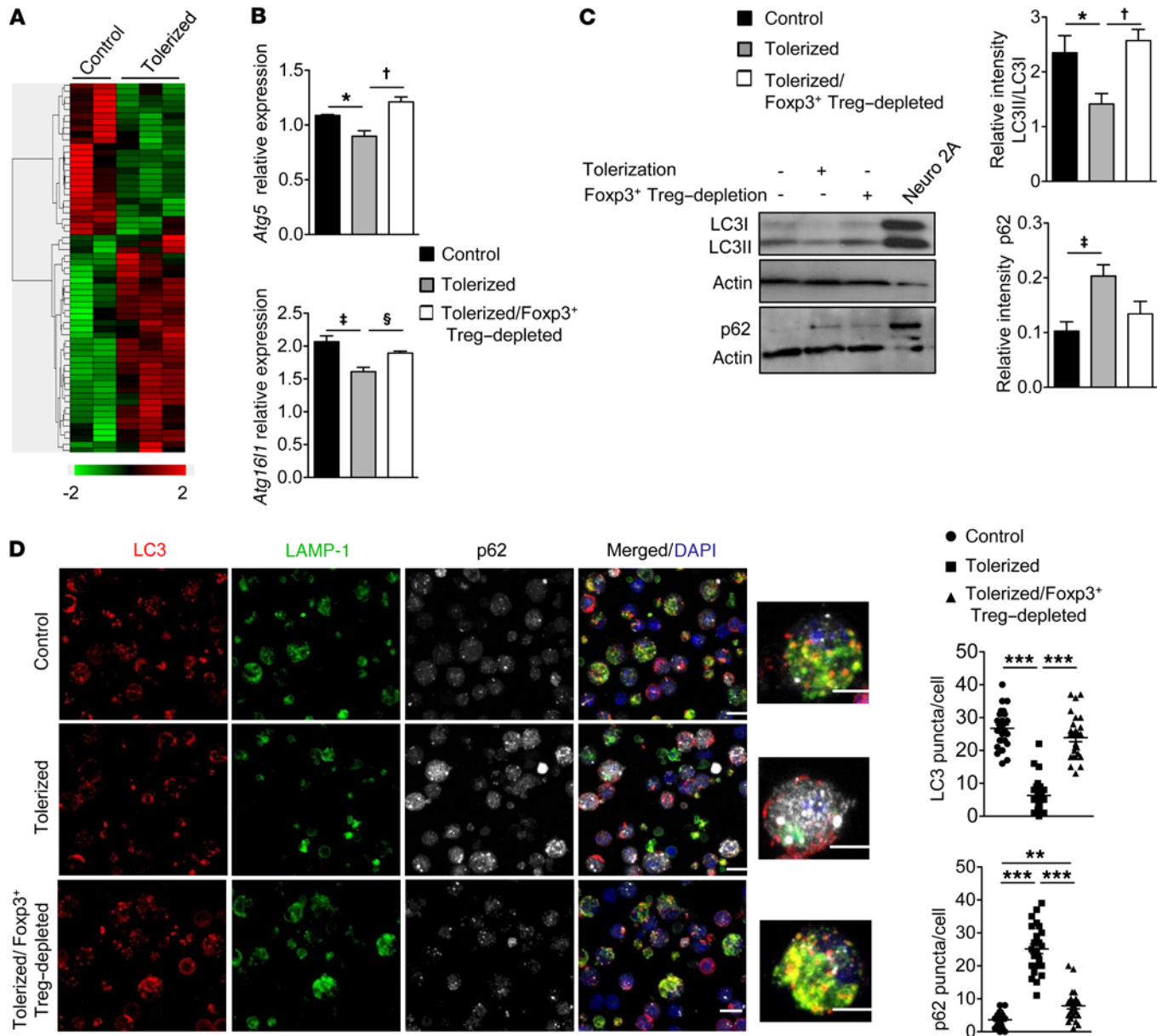
Figure 1. Foxp3+ Treg–mediated tolerance regulates autophagy in DCs. (**A**) Hierarchical clustering of autophagy-related genes upon transcriptomic analysis of sorted DCs from control (*n* = 2) and tolerized (*n* = 3) mice. (**B**) Relative mRNA expression of *Atg5* and *Atg16l1* in DCs from control, tolerized, and tolerized Foxp3+ Treg–depleted mice. Results are expressed as mean ± SEM. *n* = 6 mice per group, 3 independent experiments. **P* = 0.0389; †*P* = 0.0147; ‡*P* = 0.0145; §*P* = 0.0241. (**C**) Western blot analysis for expression of LC3, p62, and actin in DC lysates of indicated groups. Protein extract from Neuro 2A cell line was used as control. One representative experiment of 4 is depicted. Relative intensity of LC3II/LC3I and p62 are depicted. Results are expressed as mean ± SEM. *n* = 6 mice per group, 3 independent experiments. **P* = 0.0184; †*P* = 0.05; ‡*P* = 0.0432. (**D**) Immunofluorescence confocal microscopy for LC3 (red), LAMP-1 (green), p62 (silver white), and DAPI (blue) in DCs. Representative fields at 2 different magnifications are depicted. Scale bars: 5 μm. One representative experiment of 3 is shown. *n* = 4 mice per group. LC3 puncta/cell and p62 puncta/cell are depicted. ***P < 0.0001; **P = 0.0003. Results are expressed as mean ± SEM. *n* = 4 mice per group, 3 independent experiments. For **A**–**D**, DCs were isolated from dLNs and spleens of mice at 3.5 days after immunization. Statistical significance was obtained by 2-way ANOVA.

unit of PI3K, and Akt compared with DC lysates from Foxp3⁻ T cell–transferred animals (Figure 2B). Furthermore, activation of mTOR leads to phosphorylation of the ribosomal protein S6 and phosphorylation of the eukaryotic initiation factor 4E-binding protein 1 (4EBP1). DCs from Foxp3+ Treg–transferred mice demonstrated increased phosphorylation of S6 and 4EBP1 (Figure 2C), confirming the activation of the mTORC1 signaling pathway in Foxp3+ Treg–exposed DCs.

Canonical autophagy requires activation of the preinitiation complex, comprising ULK-1/2, FIP200, and ATG13 (31, 32). Accordingly, the phosphorylation of serine/threonine kinase UNC-51–like kinase-1 (ULK-1) was significantly decreased in DC lysates isolated from Foxp3+ Treg–transferred *Rag1⁻/⁻* mice (Figure 2D). In support, immunofluorescence confocal microscopy for pULK-1 in DCs verified that Foxp3+ Treg–transferred *Rag1⁻/⁻* mice exhibited reduced phosphorylation of ULK-1 (Figure 2E).
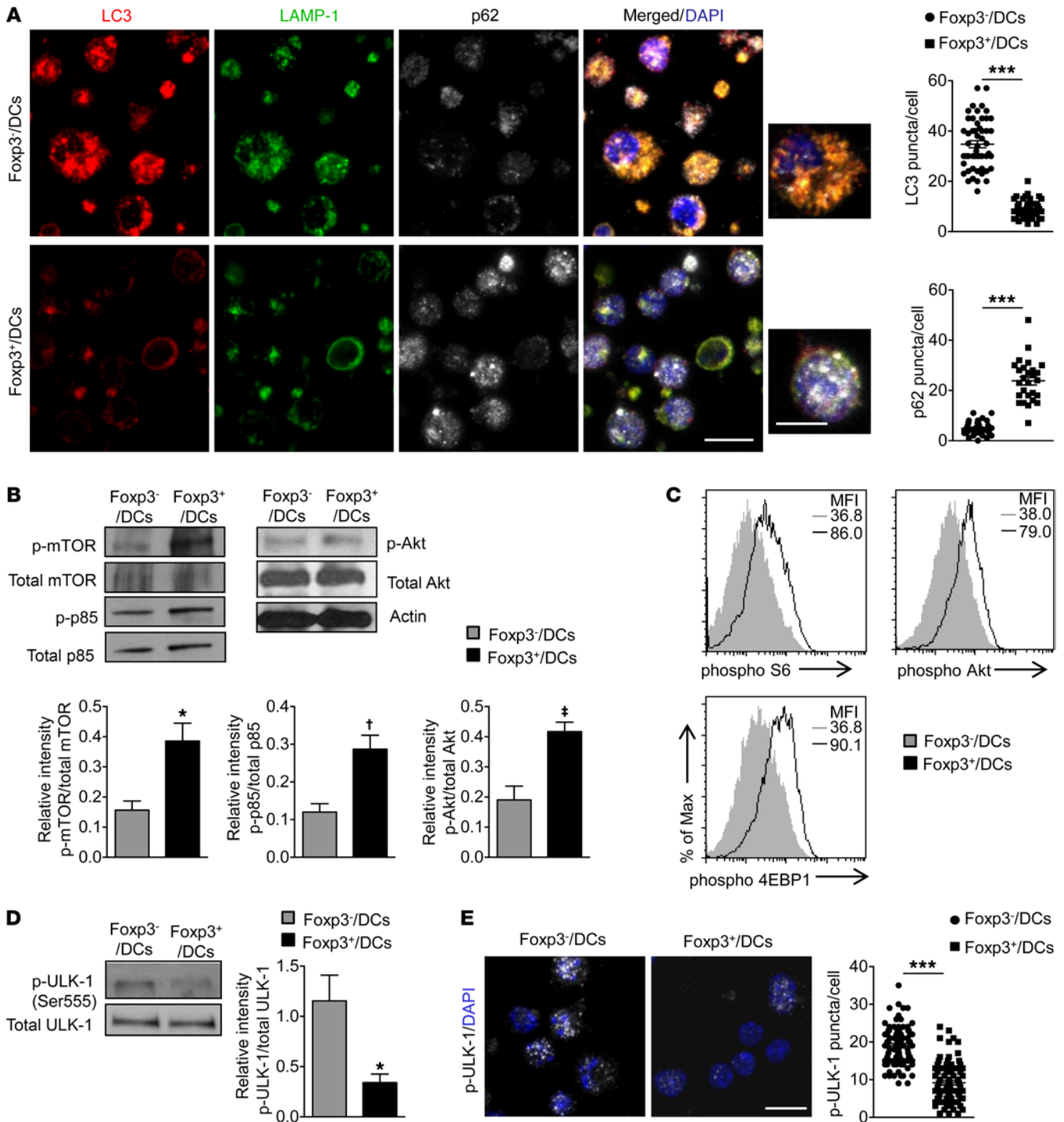
Figure 2. Foxp3+ Tregs suppress the autophagic machinery of DCs under inflammatory conditions. DCs were isolated from dLNs and spleen of *Rag1−/−* immunized mice adoptively transferred with Foxp3+ or Foxp3− CD4+ T cells. (**A**) Immunofluorescence confocal microscopy for LC3 (red), LAMP-1 (green), p62 (silver white), and DAPI (blue). Representative fields at 2 different magnifications. Scale bars: 5 μm; 10 μm (magnified). One representative experiment is shown. LC3 puncta/cell and p62 puncta/cell are depicted. ***$P < 0.0001$. (**B**) Western blot analysis for expression of p-mTOR, total mTOR, p-p85, total p85, p-Akt, and total Akt. *$P = 0.05$; †$P = 0.0241$; ‡$P = 0.0110$. (**C**) p-4EBP1, p-S6, and p-Akt expression analyzed by flow cytometry. MFI, mean fluorescence intensity. (**D**) Western blot analysis for expression of p-ULK-1 and total ULK-1. *$P = 0.0334$. (**E**) Immunofluorescence confocal microscopy for p-ULK-1 (silver white) and DAPI (blue). Scale bar: 10 μm. One representative experiment is shown. p-ULK-1 puncta/cell are depicted. ***$P < 0.0001$. For **A** and **E**, results are expressed as mean ± SEM. *n* = 4 mice per group, 3 independent experiments. Statistical significance was obtained by unpaired Student's *t* test. For **B**–**D**, 1 representative experiment of 4 is depicted.

Together, these results indicate that Foxp3$^+$ Tregs downregulate the canonical autophagy pathway in DCs.

Downmodulation of DC autophagy compromises autoantigen presentation and experimental autoimmune encephalomyelitis induction. To assess the biological significance of Foxp3$^+$ Treg–mediated diminished DC autophagy, we exposed ex vivo–isolated DCs from Foxp3$^+$ or Foxp3$^-$ T cell–transferred MOG$_{35–55}$–immunized *Rag1$^{-/-}$* mice to LPS-OVA-Fluor–coated carboxylated beads. We noticed a decreased recruitment of LC3 to antigen-containing phagosomes in DCs from Foxp3$^+$ T cell–transferred mice compared with those from control or Foxp3$^-$ T cell–transferred animals, as determined by the colocalization of LC3 with OVA-Fluor (Figure 3A). Furthermore, DCs isolated from Foxp3$^+$ Treg–depleted mice exposed to LPS-OVA-Fluor–coated carboxylated beads exhibited enhanced LC3 recruitment to antigen-containing phagosomes compared with DCs from immunized mice (Supplemental Figure 3A). These results denote that, although Foxp3$^+$ Treg–exposed DCs have normal antigen uptake ability, their autophagy-dependent antigen-processing pathway is impaired. In order to investigate whether autophagy is required for DC antigen presentation, we took advantage of the YAe Ab that reacts with a class II MHC self-Ea$_{52–68}$ peptide bound to I-A^b molecules. DCs from *Atg16l1$^{fl/fl}$ Cd11c-Cre* (*Atg16l1$^{\Delta Cd11c}$*) mice, which are genetically modified to specifically lack *Atg16l1* (33), presented less Ea peptide on their surface compared with control *Atg16l1$^{fl/fl}$* DCs (Supplemental Figure 3B), confirming that formation of mature autophagosomes is required for DCs to efficiently present peptides on MHC II molecules.

Next, we sought to examine how diminished DC autophagy affects T cell responses. Treatment of MOG$_{35–55}$ peptide–pulsed DCs with NH$_4$Cl that inhibits fusion of autophagosomes with lysosomes (Figure 3B) or the PI3K inhibitor Wortmannin (WM) (Supplemental Figure 3C) showed decreased potential toward the proliferation of MOG$_{35–55}$–specific T cells (Vα3.2$^+$Vβ8.1$^+$CD4$^+$ cells) isolated from 2D2 TCR transgenic mice (Figure 3B and Supplemental Figure 3C). In line with this, treatment of MOG$_{35–55}$–pulsed DCs with MRT$_{67307}$, which specifically inhibits UKL1 (34), markedly suppressed 2D2 T cell proliferation (Figure 3C). Importantly, T cell activation and proliferation as well as IL-2 secretion were significantly inhibited in DCs isolated from *Atg16l1$^{\Delta Cd11c}$* mice as compared with DCs isolated from *Atg16l1$^{fl/fl}$* littermate controls (Figure 3D). These results demonstrate that inhibiting autophagosome formation or autophagosomal function in DCs impaired their ability to induce antigen-specific T cell responses in vitro.

To examine whether autophagy is required for antigen processing and loading to the MHC II compartment, we isolated *Atg16l1*-deficient or -competent DCs, pulsed them with OVA whole protein, and assessed their ability to induce antigen-specific proliferation in Vα2$^+$CD4$^+$CD25$^-$ OT-II T cells. Importantly, DCs from *Atg16l1$^{\Delta Cd11c}$* mice induced significantly less OVA-specific T cell activation and proliferation of OT-II T cells as compared with control *Atg16l1$^{fl/fl}$* DCs (Figure 3E). Our findings demonstrate that canonical autophagy is required for competent antigen presentation by DCs.

To address whether downmodulation of DC autophagy compromises autoantigen presentation, we developed a protocol for experimental autoimmune encephalomyelitis (EAE) induction by transferring 2D2 MOG$_{35–55}$ antigen–specific T cells along with *Atg16l1$^{\Delta Cd11c}$* or *Atg16l1$^{fl/fl}$* DCs into *Rag1$^{-/-}$* mice (Figure 3F). Strikingly, *Atg16l1*-deficient DCs induced significantly less severe EAE disease compared with *Atg16l1$^{fl/fl}$* DCs, as denoted by disease score (Figure 3G) and disease incidence (Supplemental Table 1) as well as diminished mononuclear cell infiltration into the spinal cord (Figure 3H). Overall, our results reveal that restrained DC autophagy results in impaired autoantigen presentation and diminished autoreactive T cell priming as well as autoimmune disease induction.

Foxp3$^+$ Tregs inhibit autophagy in DCs in a CTLA4-dependent manner. To elucidate the molecular mechanism underlying the Treg-mediated inhibition of autophagy in DCs, we initially focused on IL-10, which has been associated with Foxp3$^+$ Treg suppressive function (35). Adoptive transfer of IL-10–deficient (*Il10$^{-/-}$*) Tregs (CD4$^+$CD25^{hi}) into syngeneic MOG$_{35–55}$–immunized *Rag1$^{-/-}$* animals demonstrated a significant reduction of autophagosome formation, based on LC3II and increased expression of p62 in DC protein lysates, similar to DC lysates prepared from *Il10$^{+/+}$* Treg transferred mice (Supplemental Figure 4A). These data indicate that Tregs modulate autophagy in DCs in an IL-10–independent manner.

Since expression of CTLA4 by Foxp3$^+$ Tregs has been closely linked to their suppressive function both in vitro and in vivo (3, 7), we assessed whether CTLA4 was involved in Foxp3$^+$ Treg–mediated inhibition of DC autophagy. To this end, upon blockade of CTLA4 during the in vitro coculture assay described in Supplemental Figure 2A, Tregs lost their ability to suppress the autophagosome formation in DCs, as indicated by augmented LC3-GFP expression (Figure 4A). Notably, assessment of autophagy in OVA$_{323–339}$–pulsed DCs isolated from *B7.1 B7.2* double-knockout animals and cocultured with OT-II Tregs revealed significantly increased levels of LC3 puncta compared with WT DCs, indicating that B7 molecule engagement by Tregs is required for inhibition of autophagy (Supplemental Figure 4B).

Importantly, in vivo administration of CTLA4 blocking mAbs during the adoptive transfer of Foxp3$^+$ Tregs in MOG$_{35–55}$–immunized *Rag1$^{-/-}$* animals demonstrated significantly increased induction of autophagy based on LC3 lipidation and reduced expression of p62 in DC lysates as compared with control DCs (Figure 4B). Consistently, immunofluorescence confocal microscopy revealed increased formation of autophagolysosomes in anti-CTLA4–treated Foxp3$^+$/DCs as compared with Foxp3$^+$/DCs (Figure 4C). Finally, adoptive transfer of Tregs sorted from spleen and LNs of tamoxifen-treated *Ctla4* inducible knockout mice (*Rosa26-Cre$^{ERT2+/-}$ Ctla4$^{fl/fl}$* mice, designated as CTLA4 iKO) (36) into *Rag1$^{-/-}$* mice failed to inhibit autophagy in DCs as compared with Tregs isolated from tamoxifen-treated *Rosa26-Cre$^{ERT2-/-}$ Ctla4$^{fl/fl}$* (WT) littermates (Figure 4D).

To elucidate the mechanism of CTLA4-mediated suppression of autophagy in DCs, we first assessed the expression of autophagy-related genes in CTLA4-Ig–treated bone marrow–derived DCs (BMDCs), which showed significantly downregulated levels of *Atg5*, *Atg16l1*, and *Becn1* compared with isotype-treated cells (Figure 5A). In addition, autophagolysosome formation was markedly decreased following treatment with CTLA4-Ig, as denoted by the reduced LC3 localization to the lysosomes and the significantly increased accumulation of p62 (Figure 5B). In support, impaired autophagic flux was observed upon treatment of CTLA4-Ig–exposed DCs with the lysomotropic chloroquine or the vacuolar
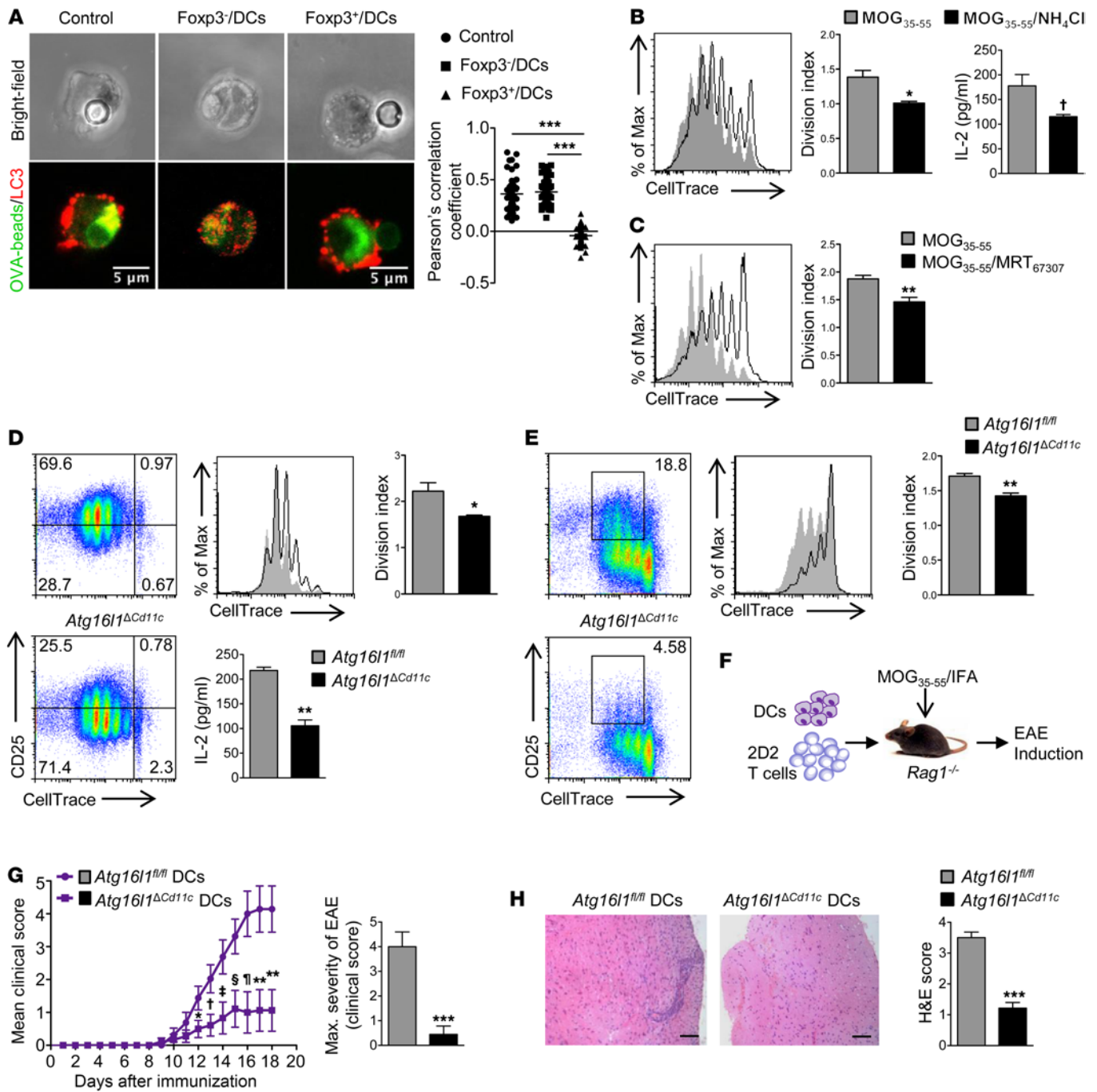
Figure 3. Restrained DC autophagy impairs antigen presentation and CD4⁺ T cell responses. (**A**) Carboxylated beads conjugated to LPS/OVA-Fluor (green) were internalized by DCs from *Rag1*⁻/⁻ immunized mice adoptively transferred with Foxp3⁺ or Foxp3⁻CD4⁺ T cells and analyzed for LC3 (red). ***$P < 0.0001$, Pearson's correlation coefficient. Representative images from 3 experiments Scale bars: 5 μm. (**B** and **C**) DCs from naive mice were treated with LPS and MOG$_{35-55}$ in the presence or absence of NH$_4$Cl (**B**) or MRT$_{37607}$ (**C**) for 4 hours and cultured with CellTrace-labeled 2D2 T cells. Cell-Trace dilution and division index are shown. *$P = 0.0187$; **$P = 0.0070$; †$P = 0.0363$. (**D**) DCs from *Atg16l1*^{ΔCd11c} or *Atg16l1*$^{fl/fl}$ MOG$_{35-55}$–immunized mice were pulsed with MOG$_{35-55}$ for 4 hours and cultured with CellTrace-labeled 2D2 T cells. CellTrace dilution and division index are shown. *$P = 0.0438$; **$P = 0.0012$. (**E**) DCs from *Atg16l1*^{ΔCd11c} or *Atg16l1*$^{fl/fl}$ mice were pulsed with OVA protein for 18 hours and cultured with CellTrace-labeled OT-II T cells. CellTrace dilution and division index are shown. Representative images from 3 experiments. **$P = 0.0073$. (**F**) Experimental design for EAE induction upon adoptive transfer of DCs from *Atg16l1*^{ΔCd11c} or *Atg16l1*$^{fl/fl}$ mice and 2D2 T cells into *Rag1*⁻/⁻ mice. (**G**) Mean clinical score and EAE severity. *$P = 0.0494$; †$P = 0.0180$; ‡$P = 0.0196$; §$P = 0.0121$; ¶$P = 0.0066$; **$P = 0.0061$; ***$P < 0.0001$. (**H**) Representative H&E sections from spinal cords of *Atg16l1*^{ΔCd11c} (clinical score 3.5) and *Atg16l1*$^{fl/fl}$ (clinical score 1.5) mice at 14 days after immunization. ***$P < 0.0001$. Results are expressed as mean ± SEM. $n = 4$ mice per group. Statistical significance was obtained by unpaired Student's t test (**B–H**) or 2-way ANOVA (**A**).
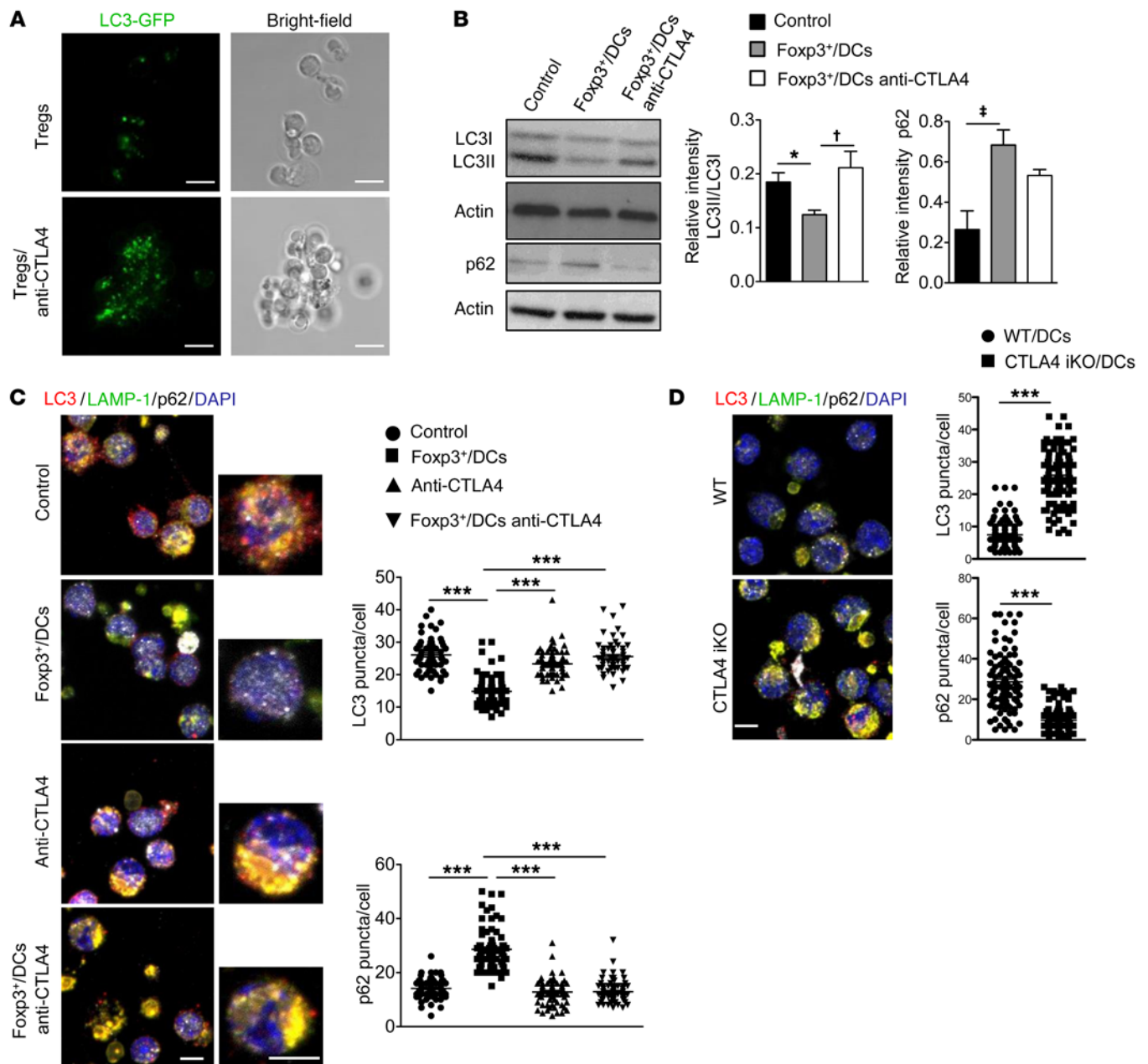
Figure 4. Foxp3+ Tregs modulate macroautophagy in DCs in a CTLA4-dependent fashion. (**A**) Confocal microscopy for cocultures of OVA-specific OT-II Tregs with sorted DCs from syngeneic LC3-GFP mice in the presence of OVA$_{323-339}$ peptide and anti-CTLA4 mAbs. Representative images from 3 individual experiments are depicted. Scale bars: 10 μm. (**B**) Western blot analysis for LC3, p62, and actin in DC lysates of indicated groups. One representative experiment of 3 is depicted. Relative intensities of LC3II/LC3I and p62 are depicted. Results are expressed as mean ± SEM. $n = 6$ mice per group, 3 independent experiments. *$P = 0.0290$; †$P = 0.0341$; ‡$P = 0.0392$. (**C** and **D**) Immunofluorescence confocal microscopy for LC3 (red), LAMP-1 (green), p62 (silver white), and DAPI (blue) in DCs isolated from dLNs and spleen of (**C**) Foxp3+ transferred *Rag1*$^{-/-}$ mice or (**D**) CTLA4 iKO or control littermate mice. LC3 and p62 puncta/cell are depicted. Representative fields in 2 different magnifications are depicted. Scale bars: 5 μm. ***$P < 0.0001$. One representative experiment of 3 is shown. Results are expressed as mean ± SEM. $n = 4$ mice per group, 3 independent experiments. Statistical significance was obtained by 2-way ANOVA (**B** and **C**) or unpaired Student's *t* test (**D**).

ATPase inhibitor bafilomycin A1 (ref. 37 and Figure 5C). In terms of function, CTLA4-Ig–treated DCs pulsed with MOG$_{35-55}$ peptide demonstrated reduced potential to promote proliferation of 2D2 T cells in vitro (Supplemental Figure 5A) and this was accompanied by reduced expression of IA^b and CD80/CD86 molecules (Supplemental Figure 5B) compared with IgG-treated DCs. Mechanistically, engagement of CTLA4-Ig on BMDCs demon-

strated increased phosphorylation of S6, 4EBP1, and Akt (Figure 5D) and reduced phosphorylation of ULK-1 (Supplemental Figure 5C). Selective inhibition of PI3K signaling (Ly294002) inhibited Akt and mTOR phosphorylation (Supplemental Figure 6A), augmented autophagolysosomal degradation (Supplemental Figure 6B), and rescued the decreased proliferation of 2D2 CD4+ T cells in vitro (Supplemental Figure 6C) in CTLA4-Ig–treated DCs.

Importantly, CTLA4-Ig–treated DCs from *Pik3cg$^{-/-}$* mice, which lack the catalytic γ subunit of PI3K (38), showed attenuated potential to induce the proliferation of 2D2 CD4$^+$ T cells in vitro compared with Ig-treated *Pik3cg$^{-/-}$* DCs (Figure 5E), confirming that CTLA4-mediated inhibition of autophagy on DCs is via the PI3K/Akt/mTOR axis. Finally, serum starvation resulted in significantly increased levels of autophagy in CTLA4-Ig–treated DCs, indicating that alternative activation of autophagy could overcome the CTLA4-Ig–mediated effect (Supplemental Figure 6D). In support, CTLA4-Ig–treated/serum-starved MOG$_{35–55}$–pulsed BMDCs demonstrated greater potential to promote 2D2 CD4$^+$ T cell proliferation as compared with CTLA4-Ig–treated MOG$_{35–55}$–pulsed control BMDCs, suggesting that alternative activation of autophagy in CTLA4-Ig–treated DCs also affects their antigen presentation potential (Supplemental Figure 6E).

To examine whether CTLA4-Ig–mediated inhibition of autophagy to DCs is through B7.1 or B7.2 molecules, BMDCs were pretreated with blocking anti-B7.1, anti-B7.2, or both prior to CTLA4-Ig addition. Our results demonstrate that blocking the interaction of CTLA4 with B7.1 and/or B7.2 significantly enhanced DC autophagy, indicating that CTLA4-mediated inhibition of autophagy in DCs is via B7.1/B7.2 molecules (Figure 5F). Notably, treatment of BMDCs with CD28-Ig did not impair the autophagy pathway, suggesting that autophagy inhibition in DCs was specific to CTLA4 ligation (Figure 5G).

CTLA4 engagement induces FoxO1 nuclear exclusion and downregulation of Lc3b transcription. We next sought to determine the molecular events involved in the CTLA4-mediated inhibition of autophagy in DCs. Crosslinking of CD80/CD86 in human DCs has been demonstrated to activate the PI3K/Akt pathway (39). To this end, immunoprecipitation of PI3K-containing complexes in DCs isolated from Foxp3$^+$ Treg–transferred MOG$_{35–55}$–immunized *Rag1$^{-/-}$* mice demonstrated interaction between CD86 and p85, the catalytic subunit of PI3K (Figure 6A), whereas low levels of interaction were observed in DCs isolated from control mice (MOG$_{35–55}$/CFA–immunized *Rag1$^{-/-}$* mice), suggesting that binding to CD86 can directly activate the PI3K pathway. The fact that the FoxO subfamily has been implicated in the regulation of autophagy gene transcription (40) and that our previously published transcriptomic data from Treg-exposed DCs revealed FoxO1 to be markedly downregulated (−3.3-fold) prompted us to investigate whether FoxO1 is implicated in the CTLA4-mediated inhibition of DC autophagy. In support of DNA microarray data, expression of *Foxo1* was significantly decreased in CTLA4-Ig–treated DCs as compared with control DCs (Figure 6B). FoxO1 has been reported to increase transcription of *Lc3b* (41). Along this line, our results demonstrate that *Lc3b* expression levels in DCs are diminished upon CTLA4 binding (Figure 6B) and, importantly, that CTLA4-mediated signaling in DCs reduces the binding of FoxO1 to the relative sites of *Lc3b* proximal promoter compared with control DCs (Figure 6, D and E), as demonstrated by ChIP assay.

To provide additional evidence for the FoxO1-mediated transcriptional regulation of autophagy genes, we examined the compartmentalization of FoxO1, since Akt has been shown to promote phosphorylation and subsequent FoxO1 nuclear exclusion (40). To this end, Western blot analysis and confocal microscopy revealed significantly reduced protein levels of nuclear FoxO1 in CTLA4-Ig–treated DCs compared with control Ig–treated DCs (Figure 6, E and F), confirming the notion that CTLA4 binding promotes FoxO1 nuclear shuttling.

To demonstrate a direct linear relationship among CTLA4 binding, Akt-mediated FoxO1 nuclear exclusion, and inhibition of autophagy in DCs, we treated BMDCs from *Akt1$^{-/-}$* animals with CTLA4-Ig. Notably, CTLA4-Ig–treated *Akt1$^{-/-}$* BMDCs demonstrated increased autophagy levels, as determined by increased LC3II conversion (Figure 6G), and enhanced functional autophagolysosomal activity, as determined by confocal microscopy (Figure 6H). This was accompanied by nuclear inclusion of FoxO1 (Figure 6I). Finally, we took advantage of the FoxO1^{AAA} mutant form of FoxO1a, in which a substitution of specific Ser/Thr residues to Ala abrogates the Akt-mediated phosphorylation and subsequent nuclear shuttling of FoxO1. To this end, CTLA4-Ig–treated BMDCs transfected with pCMV5-FoxO1a-AAA-Myc (denoted as CTLA4 FoxO1^{AAA}) showed significantly increased autophagy levels compared with BMDCs transfected with pCMV5-FoxO1a-Myc control (denoted as CTLA4-Ig FoxO1^{WT}), indicating that decreased nuclear exclusion of FoxO1 increased the autophagy pathway operation (Figure 6J).

Collectively, our findings provide evidence for a CTLA4-Ig–mediated activation of the PI3K/Akt pathway that promotes the inactivation and nuclear exclusion of FoxO1 that in turn downregulates transcription of *Lc3b* and the autophagy pathway in DCs.

CTLA4-Ig diminishes autophagy in human DCs and promotes FoxO1 nuclear exclusion. CTLA4-Ig is a widely used biological therapy for RA and transplantation. To examine whether CTLA4-Ig treatment inhibited DC autophagy, we sorted highly pure CD14$^-$CD11c$^+$HLADR$^+$ DCs from peripheral blood mononuclear cells (PBMCs) of RA patients with residual active disease (disease activity score [DAS] > 2.8) (42) treated with CTLA4-Ig or anti–TNF-α biologics and assessed *LC3B* expression by quantitative PCR (qPCR). Notably, DCs from CTLA4-Ig–treated RA patients exhibited significantly downregulated *LC3B* gene expression levels compared with DCs isolated from anti–TNF-α–treated patients (Figure 7A). In addition, PBMC-derived DCs from healthy individuals treated with CTLA4-Ig in vitro exhibited suppressed autophagy, as demonstrated by the significantly reduced LC3 puncta and p62 degradation compared with control IgG-treated DCs (Figure 7B). In line with the mouse data, selective inhibition of PI3K signaling in CTLA4-Ig–treated DCs resulted in decreased phosphorylation of Akt and mTOR (Figure 7C), indicating that CTLA4-Ig inhibits autophagy in human DCs through the PI3K/Akt/mTOR pathway. Finally, CTLA4-Ig–treated DCs exhibited significantly reduced nuclear localization of FoxO1 compared with IgG-treated DCs (Figure 7D). Overall, these findings provide evidence for an CTLA4-Ig–mediated inhibition of the canonical pathway of autophagy in DCs.

Discussion

We provide insights into the molecular and cellular basis that underlie Foxp3$^+$ Treg–mediated suppression of an immune response. Specifically, we identify Foxp3$^+$ Tregs as targeting the autophagic machinery of DCs in a CTLA4-dependent manner. Disruption of DC autophagy severely affected their immunogenic properties and diminished their potential to transfer disease in vivo. Moreover, we reveal a CTLA4-induced reverse
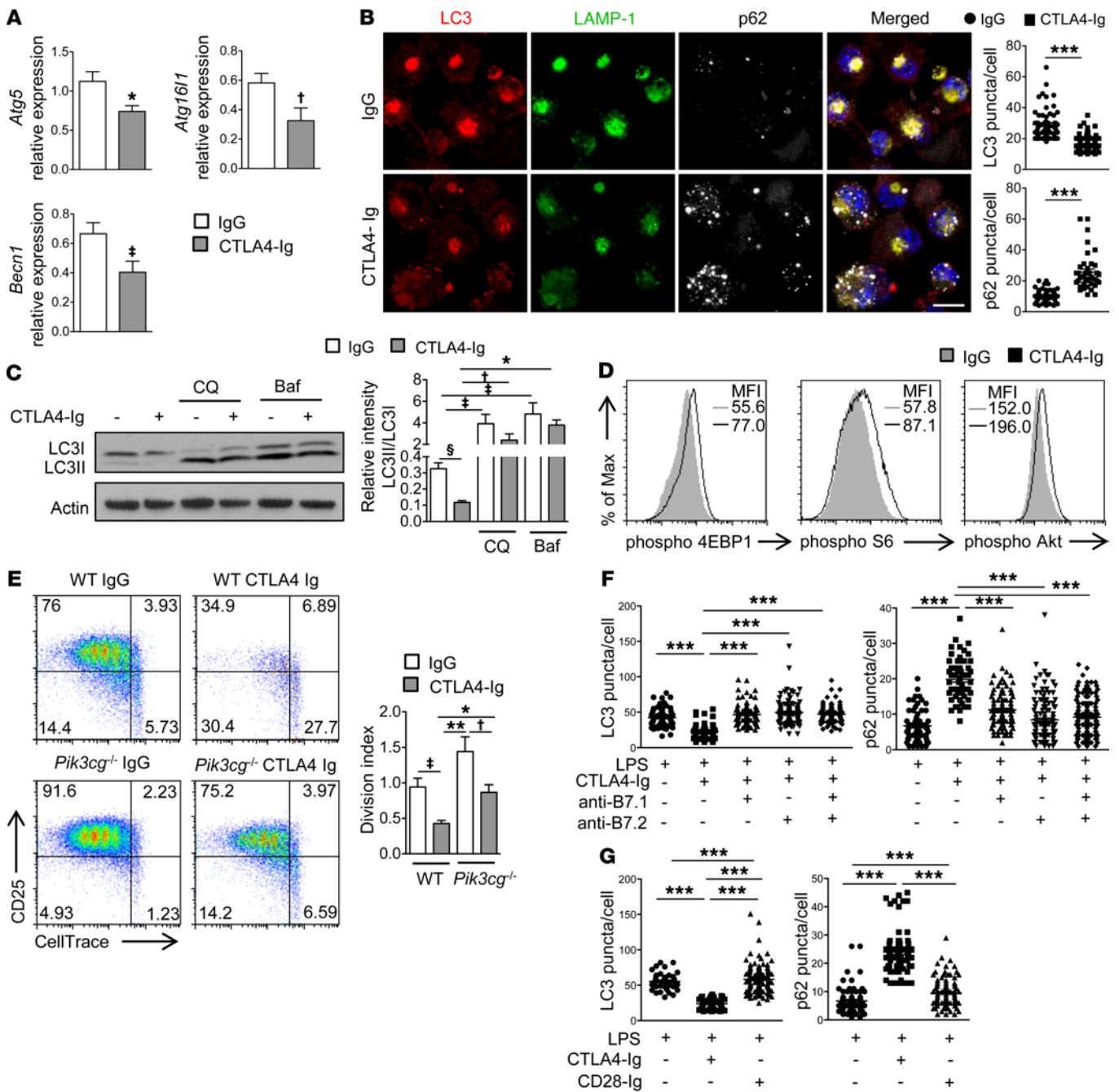
Figure 5. CTLA4 activates PI3K/Akt/mTOR signaling cascade to suppress canonical autophagy in BMDCs. BMDCs were treated with LPS, CTLA4-Ig, or IgG for 16 to 20 hours (**A**, **B**, and **D**–**H**) or 4 hours (**C**). (**A**) Relative mRNA expression of *Atg5*, *Atg16l1*, and *Becn1*. *P = 0.0432; †P = 0.0388; ‡P = 0.0390. (**B**) LC3 (red), LAMP-1 (green), p62 (silver white), and DAPI (blue). Scale bar: 10 μm. One representative experiment of 3. LC3 and p62 puncta/cell are depicted. ***P < 0.0001. (**C**) BMDCs were treated with chloroquine or bafilomycin A1 for 4 hours. Cell lysates were subjected to Western blotting for LC3 and actin. One representative experiment of 4 is shown. Relative intensity of LC3II/LC3I is depicted. *P = 0.0237; †P = 0.0491; ‡P = 0.05; §P = 0.0148. (**D**) p-4EBP1, p-S6, and p-Akt expression. One representative experiment of 4 is shown. (**E**) BMDCs from *Pik3cg*$^{-/-}$ or WT animals were treated with LPS or CTLA4-Ig for 16 hours and pulsed with MOG$_{35–55}$ for an additional 6 hours, washed, and cultured with CellTrace-labeled 2D2 T cells. CellTrace dilution, CD25 expression, and division index are depicted. One representative experiment of 5. *P = 0.0198; †P = 0.0310; **P = 0.0089; ‡P = 0.0030. (**F**) BMDCs were treated with anti-B7.1 and anti-B7.2 three hours prior to CTLA4-Ig. LC3 and p62 puncta/cell are depicted. ***P < 0.0001. (**G**) MDCs were treated with CD28 Ig for 16 to 20 hours. bLC3 and p62 puncta/cell are depicted. ***P < 0.0001. Results are expressed as mean ± SEM. n = 4–6 mice per group, 3 independent experiments. Statistical significance was obtained by unpaired Student's *t* test (**A** and **B**) or 2-way ANOVA (**C**–**G**).

signaling in DCs that activates the PI3K/Akt/mTOR axis and potentiates FoxO1 nuclear exclusion, resulting in decreased transcription of the autophagy gene *Lc3b* that is essential for autophagosome formation.

Although it is becoming apparent that the autophagic process has a great impact on almost every immunological-driven response (13), its role in the context of autoimmune diseases and, importantly, in the Foxp3$^+$ Treg–mediated induction of tol-
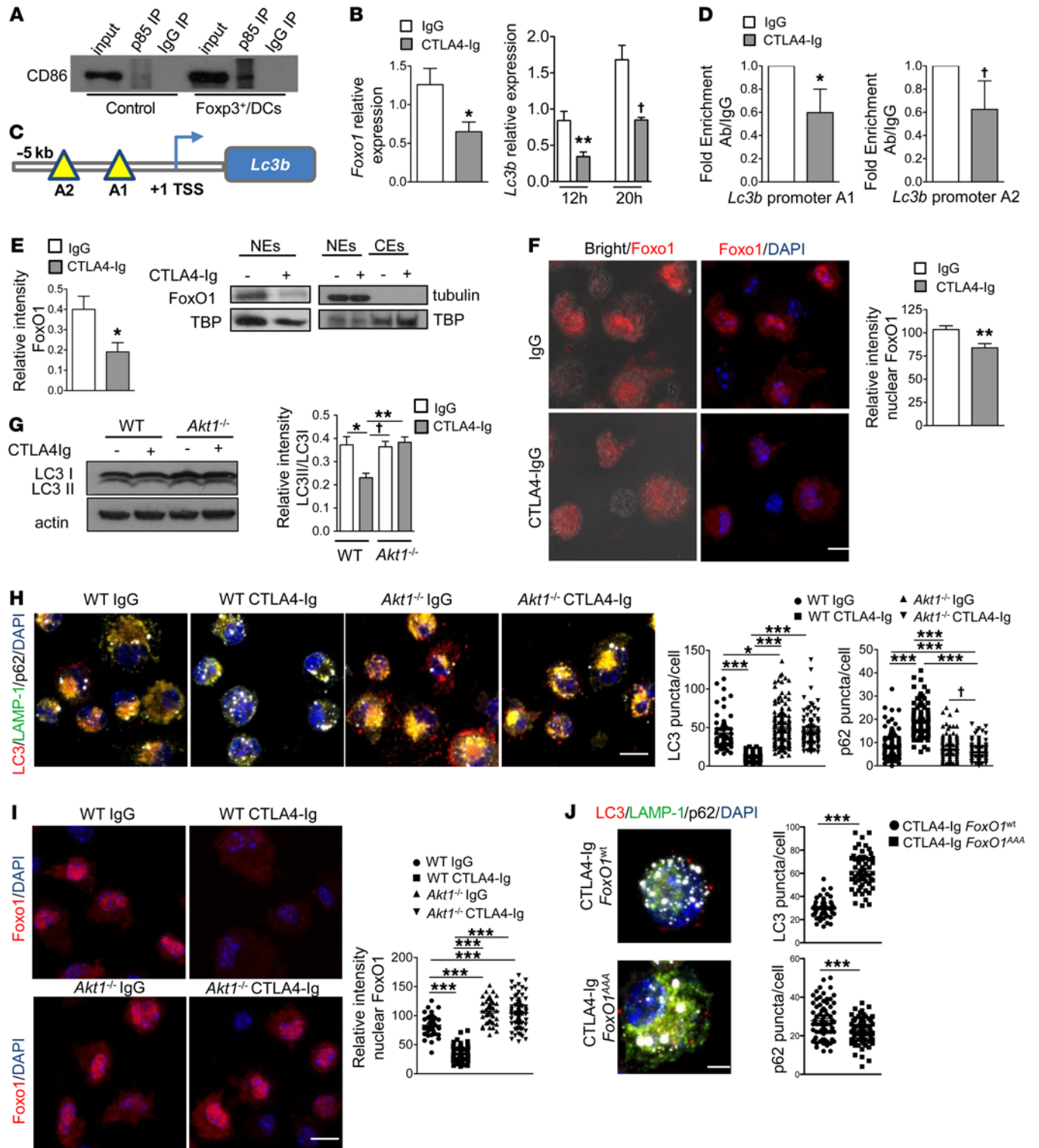
Figure 6. CTLA4-mediated nuclear exclusion of FoxO1 in DCs. (**A**) Western blot for CD86 following immunoprecipitation of p85-containing complexes in DCs from Foxp3^{+} Treg–transferred MOG$_{35-55}$–immunized $Rag1^{-/-}$ mice. (**B** and **D**) WT or $Akt1^{-/-}$ BMDCs were treated with LPS and CTLA4-Ig or IgG for 12 or 20 hours (**B** and **E**–**J**). (**B**) mRNA expression of $Foxo1$ and $Lc3b$. *P = 0.0214; **P = 0.0214; †P = 0.0023. (**C**) Schematic representation of $Lc3b$ proximal promoter with FoxO1-binding sites (A1 and A2). (**D**) ChIP analysis of the promoter of $Lc3b$ gene for FoxO1-binding sites. *P = 0.0359; †P = 0.0489. Statistical significance using paired t test. (**E**) Western blot for FoxO1, tubulin, and TBP from cytoplasmic (CEs) and nuclear (NEs) extracts. Relative intensity of FoxO1. *P = 0.0405. (**F**) FoxO1 (red), and DAPI (blue). Scale bar: 10 μm. Relative intensity of nuclear FoxO1. **P < 0.0001. (**G**) Western blot for LC3 and actin. Relative intensity of LC3II/LC3I using 2-way ANOVA. *P = 0.05; †P = 0.0291; **P = 0.0069. (**H**) LC3 (red), LAMP-1 (green), p62 (silver white), and DAPI (blue). Scale bar: 10 μm. LC3 and p62 puncta/cell are depicted. ***P < 0.0001; *P = 0,0142; †P = 0.027. (**I**) FoxO1 (red) and Dapi (blue). Scale bar: 10 μm. Relative intensity of nuclear FoxO1. ***P < 0.0001. (**J**) BMDCs were transfected with $FoxO1^{WT}$ or $FoxO1^{AAA}$. LC3 and p62 puncta/cell are depicted. Scale bar: 5 μm. ***P < 0.0001. Results are expressed as mean ± SEM. n = 4–5 mice. One representative experiment of 3 or 4 is shown. For **B**, **E**, **F**, and **H**–**J**, statistical significance was obtained by unpaired Student's t test.
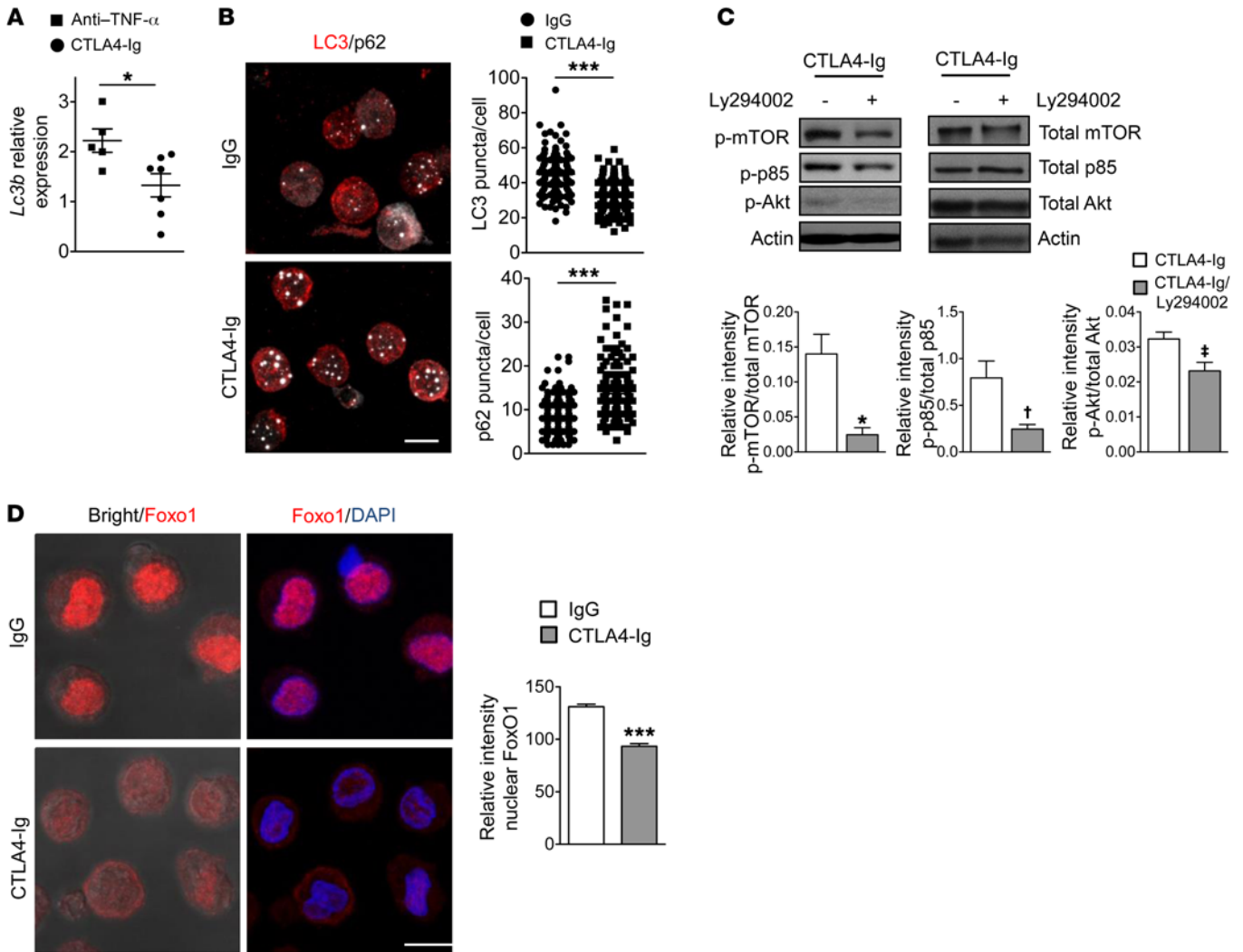
Figure 7. CTLA4-Ig diminishes autophagy pathway in human DCs and promotes FoxO1 nuclear exclusion. (A) CD11c⁺CD14⁻HLADR⁺ DCs were isolated from the periphery of anti–TNF-α–treated (n = 5) or CTLA4-Ig–treated (n = 7) RA patients (DAS > 3). Relative mRNA expression of $Lc3b$. *P = 0.0252. Results are expressed as mean ± SEM. **(B–D)** PBMCs were isolated from the periphery of healthy individuals and differentiated toward DCs in the presence of GMCSF and IL-4. DCs were treated with LPS in the presence or absence of CTLA4-Ig or Ly294002 for 16 hours. **(B)** Immunofluorescence confocal microscopy for LC3 (red) and p62 (silver white). Scale bar: 10 μm. One representative experiment of 3 is shown. LC3 puncta/cell and p62 puncta/cell are depicted. Results are expressed as mean ± SEM; n = 6 donors per group. ***P < 0.0001. **(C)** Western blot analysis for expression of p-mTOR, total mTOR, p-p85, total p85, p-Akt, and total Akt in DC lysates. One representative experiment of 3 is depicted. *P = 0.0181; †P = 0.0438; ‡P = 0.0432. **(D)** Immunofluorescence confocal microscopy for FoxO1 (red) and DAPI (blue). Scale bar: 10 μm. One representative experiment is shown. Relative intensity for nuclear FoxO1 is depicted. Results are expressed as mean ± SEM. n = 6 healthy donors per group. Statistical significance was obtained by unpaired Student's t test. ***P < 0.0001.

erance remains elusive. Our findings demonstrate that Foxp3⁺ Tregs exert their function via modulation of autophagy cascade in DCs, since Foxp3⁺ Tregs impaired autophagolysosome formation in DCs from MOG₃₅₋₅₅–immunized $Rag1^{-/-}$ mice. Accumulating data underscore an essential role of autophagy during antigen presentation by APCs and priming of adaptive immune responses (13, 14, 17–20, 43). We extended these findings by demonstrating that DCs with specific deletion of $Atg16l1$ were less efficient in promoting CD4⁺ T cell activation and proliferation in vitro compared with $Atg16l1$-sufficient DCs, and importantly, DC autophagy was required for the priming of autoreactive CD4⁺ T cells in vivo and development of EAE. This is in agreement with previous reports demonstrating that mice with $Atg7$ deficiency in DCs or myeloid cells develop milder EAE

compared with control animals. However, the direct effect of $Atg7^{-/-}$ DCs on disease development was not addressed (44, 45).

Interestingly, our results demonstrate that DC autophagy is required for the presentation of exogenous MOG₃₅₋₅₅ peptide. Previous reports have shown that APCs from H-2M knockout animals (with normal class II expression) demonstrated reduced capacity to present exogenous peptides to class II–restricted T cells (46, 47). In support, H-2M KO APCs required more than 1 log higher MOG₃₅₋₅₅ concentration to stimulate MOG₃₅₋₅₅–specific T cells in vitro and invariant chain (Ii) KO animals immunized with MOG₃₅₋₅₅ peptide failed to induce EAE (48). Finally, both Ii- and HLA-DM–deficient mice were able to prime MOG₃₅₋₅₅–specific Th1 responses, but the magnitude of the response was significantly lower compared with that of WT animals (49). In support, our findings show that treat-

ment of DCs with the lysomotropic NH_4Cl during MOG_{35-55} peptide pulsing markedly reduced their stimulatory properties in vitro. The mechanism involved in MOG_{35-55} peptide processing by DCs is currently unknown and warrants further investigation. Interestingly, peptide–MHC class II complexes are constantly being internalized in a very well-characterized ubiquitin-mediated mechanism and are transported to early endosomes and back to the plasma membrane. This is consistent with a model in which "old" MHC class II complexes in mature DCs can generate "new" peptide–MHC class II complexes following antigen internalization (50). In our model, analysis of DCs from tolerized (MOG_{35-55}–infused) animals demonstrated increased expression of the E3 ubiquitin ligase MARCH8 (our unpublished data), which regulates the turnover of peptide–MHC class II complexes (51) suggesting that decreased turnover of peptide–MHC class II complexes might take place and this could be accompanied by decreased stimulation of MOG_{35-55}–specific T cell responses. Overall, all the above suggest that MOG_{35-55} peptide serves as a macroautophagy substrate.

CTLA4 is constitutively expressed by Foxp3+ Tregs and has been shown to be instrumental for Treg-mediated suppression (3, 7). Although the molecular mechanism that underlies the CTLA4-dependent negative regulation during Treg-mediated suppression is ill defined, a cell-extrinsic function of CTLA4 through transendocytosis of costimulatory molecules of the B7 family has been proposed (9). In this regard, our in vivo data propose an additional cell-extrinsic mechanism that involves the CTLA4-mediated modulation of autophagy in DCs. It is likely that under inflammatory conditions, Foxp3+ Tregs acquire stable contacts with antigen-bearing DCs (4, 6) via CTLA4, thus modulating their autophagic machinery. In support, antigen-specific Tregs failed to suppress autophagy in antigen-pulsed B7.1 B7.2 double-knockout DCs. Finally, CTLA4-Ig has been approved for the treatment of RA in patients with inadequate response to conventional disease modifying antirheumatic drugs (DMARDs). Although several mechanisms have been proposed to explain the therapeutic potential of CTLA4-Ig (52), the precise molecular and cellular targets remain elusive. Our findings point toward a crucial role of CTLA4-Ig in the modulation of the autophagy pathway and suggest that CTLA4-Ig diminishes autophagy in DCs, rendering them less immunogenic and hence unable to potentiate autoreactive T cell responses.

The kinase mTOR is a critical regulator of macroautophagy. Foxp3+ Treg–exposed DCs displayed increased mTORC1 activity (increased phosphorylation of S6 and 4EBP1), suggesting that Foxp3+ Tregs diminish the macroautophagy pathway in DCs through activation of the PI3K/Akt/mTOR axis. Suppression of the PI3K/Akt/mTOR pathway activates autophagy though dephosphorylation of autophagy and beclin 1 regulator 1 (AMBRA1), activation of ULK-1 complex, and autophagosome formation though ATG5, ATG12, and ATG16L1 (24, 25, 31, 32). To this end, our findings clearly demonstrate that ULK-1 phosphorylation is compromised in DCs modulated by Foxp3+ Tregs, which is most consistent with a reduction in canonical autophagy (53). In line with this, treatment of MOG_{35-55}–pulsed DCs with a specific ULK-1 inhibitor impaired their ability to stimulate 2D2 CD4+ T cells in vitro. Importantly, we demonstrate that PI3K directly interacts with CD86 molecules and that CTLA4-Ig binding to CD80/CD86 in DCs activates the PI3K/

Akt/mTOR pathway, thereby suppressing autophagy. This is consistent with a recent report showing that crosslinking of CD80/CD86 in human DCs results in activation of the PI3K/Akt pathway (39). Of interest, in the same study, ligation of CD28-Ig markedly induced p85 phosphorylation (38), whereas our results demonstrate that the autophagy pathway was not affected upon treatment of BMDCs with CD28-Ig. A possible explanation would be that integration of other pathways (i.e., the NOTCH pathway) might coregulate the biological outcome of CD28-Ig interaction, but this remains to be investigated. Our results also shed light on the controversy regarding the reverse signaling of CTLA4 to DCs. While some reports have demonstrated IDO expression by DCs upon CTLA4-Ig triggering, others have argued against this mainly in human DCs (12). In contrast to our human data, an earlier report demonstrated that treatment of APCs with CTLA4-Ig induced minimal transcriptional changes, while belatacept (a CTLA4-Ig with no mutations in the Fc portion) failed to induce transcriptional responses (54). This discrepancy could reflect the short exposure of APCs to CTLA4-Ig or the different conditions of human APC preparation.

Our findings provide evidence for a CTLA4-mediated transcriptional-dependent regulation of autophagy in DCs though activation of the PI3K/Akt axis that results in nuclear exclusion of FoxO1 and decreased transcription of Lc3b. Nuclear presence of FoxO1 is a prerequisite for transcriptional activation of autophagy genes in a process that is controlled by Akt (55). In line with this, another member of the FoxO family, FoxO3, has been shown to transactivate the expression of the Lc3 gene in cardiomyocytes (56). However, it was later delineated that FoxO3 upregulated the PI3K/Akt pathway, which phosphorylated FoxO1 and mediated FoxO1 shuttling from the nucleus (55). Interestingly, and in contrast with our results, earlier reports showed that CTLA4 binding induced FoxO3 nuclear localization in DCs (57, 58), but both studies did not provide a linear relationship between CTLA4 engagement and FoxO3 nuclear localization in DCs. Furthermore, the functional properties of DCs were studied on FoxO3 total knockout cells that failed to distinguish between nuclear and cytoplasmic FoxO3 localization. Our findings provide direct evidence for a CTLA-4–mediated activation of Akt that promotes DC FoxO1 nuclear exclusion. In line with our data, Koorella et al. demonstrated that binding to CD80/CD86 activates the PI3K/Akt pathway in human DCs (39). Subsequently, activated Akt phosphorylates FoxO3 and drives its exit from the nucleus, abrogating the FoxO3 repressive role in IL-6 expression. Importantly, studies on differential regulation of FoxO family members propose a distinct mechanism through which FoxO1 subcellular localization is mediated by Akt1 (59). This is consistent with our results, since CTLA4-Ig treatment in $Akt1^{-/-}$ DCs failed to promote FoxO1 nuclear shuttling and to suppress the autophagy pathway. Of interest, cytosolic FoxO1 was demonstrated to interact with ATG7 and to promote autophagy in immature NK cells. Unexpectedly, in cells in which the ATG7-binding domain was deleted from FoxO1, assessment of autophagy was based only on the fluorescence intensity of LC3 (LC3-GFP), which cannot adequately assess the operation of a functional autophagy pathway (60). Furthermore, autophagy in iNKs was not dependent on mTOR signaling, and the authors concluded that the autophagic activity of FoxO1 is independent of transcriptional activation

of its target genes (60). It is plausible, therefore, that different cell-dependent functions of FoxO proteins dictate outcomes on the autophagy pathway.

In summary, our results provide evidence for the operation of an in vivo mechanism during Foxp3$^+$ Treg–mediated induction of self-tolerance via modulation of autophagy in antigen-bearing DCs in the dLNs, a process that is dependent on CTLA4 expression by Foxp3$^+$ Tregs. It is plausible that Foxp3$^+$ Tregs, by targeting the autophagic machinery of DCs, diminish their immunogenicity, contributing to reestablishment of self-tolerance. Our data shed light on the mechanism of Foxp3$^+$ Treg–mediated suppression in an autoimmune environment and propose pathways toward the design of effective Treg-based immunotherapies for autoimmune diseases.

Methods

Mice. C57BL/6, *Rag1$^{-/-}$* (C57BL/6 background), *Il10$^{-/-}$* (C57BL/6 background), and OVA-TCR–transgenic OT-II mice were purchased from Jackson Laboratory. DEREG (C57BL/6 background) mice were provided by Tim Sparwasser (Institute of Infection Immunology, TWINCORE). *Foxp3-Gfp* KI mice (C57BL/6 background) were provided by Alexander Rudensky (Department of Immunology, Memorial Sloan-Kettering Cancer Center, New York, New York, USA). 2D2 TCR Tg mice were provided by Lesley Probert (Hellenic Pasteur Institute, Athens, Greece). LC3-GFP transgenic mice were from RIKEN BRC. *Atg16l1$^{\Delta Cd11c}$* mice and littermate *Atg16l1$^{fl/fl}$* control mice used in experiments were provided by Kenneth Cadwell (New York University School of Medicine) and were generated from *Atg16l1$^{fl/fl}$* and *Atg16l1$^{fl/fl}$ Cd11c-Cre* breeding pairs in which 1 parent was hemizygous for the *Cre* allele (33). *Rosa26-Cre$^{ERT2+/-}$ Ctla4$^{fl/fl}$* (CTLA4 iKO) mice and *Rosa26-Cre$^{ERT2-/-}$ Ctla4$^{fl/fl}$* (WT) mice were provided by Kajsa Wing (Karolinska Institute) and were generated by intercrossing *Ctla4* floxed and *Rosa26-Cre^{ERT2+}* mice. All mice used in the experiments were 8- to 10-week-old females.

In vivo tolerization protocol. Tolerance was induced by peptide infusion as described (22). Specifically, mice were implanted s.c. with osmotic micropumps (Alzet 1002; Durect) infusing 10 μg per day of MOG$_{35-55}$ peptide (Genemed Synthesis) for 14 days. Mice were subsequently immunized s.c. at the base of the tail with 100 μg MOG$_{35-55}$ emulsified (1:1) in CFA (Sigma-Aldrich). For depletion of Tregs, DEREG mice received i.p. 1 μg DT (Sigma-Aldrich, following completion of MOG$_{35-55}$ infusion and were immunized with MOG$_{35-55}$/CFA 5 days later.

Flow cytometry and cell sorting. Single-cell suspensions were prepared from tissues and live cells (7AAD, BD Biosciences) and were stained with conjugated Abs to mouse CD11c (N418), CD11b (M1/70), Gr-1 (RB6-8C5), Vα3.2 (RR 3-16), Vβ11 (KT11), CD25 (3C7), GITR (DTA-1; BioLegend), Va2 (B20.1), Ea$_{52-68}$ peptide bound to I-A^b (YAe; eBioY-Ae), pAkt (S473, SDRNR), pS6 (S235/236, cupk43k), p4E-BP1 (T36/T45, V3NTY24; eBioscience Inc.). These were also stained to human HLA-DR (LT-DR), CD14 (18D11), and CD11c (BU15; Immuno-Tools). For isolation of DCs, Tregs, antigen-specific T cells, and phospho-protein staining, see Supplemental Experimental Procedures.

Adoptive transfer experiments. For adoptive transfer in *Rag1$^{-/-}$* mice, 1×10^6 CD4$^+$Foxp3$^+$ or CD4$^+$Foxp3$^-$, or CD4$^+$CD25^{hi} *Il10$^{-/-}$* or *Il10$^{+/+}$* sorted cells were transferred i.v. followed by MOG$_{35-55}$/CFA immunization. In some experiments, 150 μg anti-CTLA4 mAbs (4F10) were i.p. injected at the time of Foxp3$^+$ Treg injection and 2 days later. DCs were isolated 3.5 days later.

For adoptive transfer of CTLA4-depleted Tregs, *Rosa26-Cre$^{ERT2+/-}$ Ctla4$^{fl/fl}$* (CTLA4 iKO) and *Rosa26-Cre$^{ERT2-/-}$ Ctla4$^{fl/fl}$* (WT) mice were i.p. injected with 4 mg tamoxifen in corn oil (+5% [vol/vol] ethanol) on days 0, 1, and 5. Complete depletion was achieved by day 6. On day 6, CD4$^+$CD25^{hi}GITR$^+$ Tregs were sorted from spleens and LNs of mice and adoptively transferred (1×10^6 cells) i.v. to *Rag1$^{-/-}$* mice followed by MOG$_{35-55}$/CFA immunization. DCs were isolated 3.5 days later.

For EAE induction, DCs isolated from spleens and LNs of *Atg16l1$^{fl/fl}$* or *Atg16l1$^{\Delta Cd11c}$* mice were pulsed with 25 μg/ml MOG$_{35-55}$ for 4 hours. 3×10^6 DCs, along with 5×10^6 2D2 T cells, were adoptively transferred in *Rag1$^{-/-}$* mice. Mice were subsequently immunized s.c. at the base of the tail and the flank with 200 μg MOG$_{35-55}$ in IFA (Sigma-Aldrich). Mice also received i.p. injections of 300 ng pertussis toxin (Sigma-Aldrich) at the time of immunization and 48 hours later. Mice were monitored daily for clinical signs of disease as described (61).

In vitro coculture experiments for autophagy assessment. For antigen-specific T cell DC coculture experiments, highly pure antigen-specific Tn (5×10^4) or Tregs (5×10^4) or a mixture of Tn/Tregs (4:1 ratio, 5×10^4:1.25×10^4) sorted from OT-II mice as described above were cultured with CD11c$^+$ DCs (2×10^4) isolated from syngeneic LC3-GFP or *B7.1 B7.2* double-knockout mice in the presence of OVA$_{323-339}$ peptide (10 μg/ml). In some experiments, 100 μg/ml anti–CTLA-4 mAb (4F10) was added to cultures. After 18 to 24 hours, cells were gently transferred to a Lab-Tek chambered 1.0 borosilicone coverglass system (Thermo Scientific). In other experiments, DCs were resorted from the cultures and stained for LC3 and DAPI. Cells were visualized using inverted confocal live cell imaging system Leica SP5.

Histological analysis and immunofluorescence. H&E sections of spinal cord were performed as described (22). For autophagy immunofluorescence, phagocytosis, and immunofluorescence, refer to Supplemental Experimental Procedures.

Generation of BMDCs. BMDCs were generated following an established protocol (62). At day 9, cells were pulsed with 0.5 μg/ml LPS in the presence of 100 μg/ml CTLA4-Ig (Bristol-Myers Squibb) or 2 μg/ml recombinant mouse CD28-Ig (BioLegend) and collected 12 or 16 to 20 hours later. In some experiments, cells were treated with 20 μM Ly294002 (Cell Signaling) for 16 hours. BMs from *Akt1$^{-/-}$* mice were provided by C. Tsatsanis (Medical School, University of Crete, Crete, Greece). BMs from *Pik3cg$^{-/-}$* mice were provided by A. Ghigo (Molecular Biotechnology Center, University of Torino).

In other experiments, BMDCs were treated with 0.5 μg/ml LPS in the presence or absence of Abs against B7.1 (HB301) or B7.2 (HB-253). Three hours later, 100 μg/ml CTLA4-Ig was added to the culture for an additional 16 hours.

For FoxO1^{AAA} transfection experiments, BMDCS were transfected using Lipofectamine 2000 (Invitrogen) with 2.5 μg of plasmid DNA, either pCMV5-mFoxO1a(WT)-Myc (plasmid 12142) or pCMVm-FoxO1a(AAA)-Myc-HA (plasmid 17547) (Addgene). Plasmid DNA was mixed with Lipofectamine followed by 20 minutes incubation and then added to cells according to the manufacturer's instructions. Cells were washed after 4 hours, and medium was refreshed. After 48 hours, BMDCs were pulsed with 0.5 μg/ml LPS in the presence of 100 μg/ml CTLA4-Ig.

T cell proliferation assays and cytokine assessment. BMDCs were pulsed with 20 μg/ml MOG$_{35-55}$ peptide in the presence or absence of 100 nM Wortmannin (Sigma-Aldrich) for 6 hours. In other experiments, DCs isolated from LNs and spleens of naive C57BL/6 mice were treated with 0.5 μg/ml LPS and 25 μg/ml MOG$_{35-55}$ in the pres-

ence or absence of 20 mM NH₄Cl, 75 μM MRT$_{67307}$ (Tocris), or 20 μM Ly294002 (Cell Signaling). In some experiments, DCs were isolated from spleens and LNs of *Atg16l1$^{fl/fl}$* or *Atg16l1^{ΔCd11c}*–MOG$_{35–55}$–immunized mice and pulsed with 25 μg/ml MOG$_{35–55}$ for 4 hours. $5 × 10^4$ DCs were cultured with $10 × 10^4$ CellTrace-labeled (Invitrogen) 2D2 T cells. Proliferation was assessed 72 hours later. In other experiments, DCs were isolated from spleens and LNs of *Atg16l1$^{fl/fl}$* or *Atg16l1^{ΔCd11c}* mice and pulsed with 50 μg/ml OVA grade V (Sigma-Aldrich) in the presence of 0.5 μg/ml LPS for 16 hours. $10 × 10^4$ DCs were cultured at a 1:1 ratio with CellTrace-labeled OT-II T cells. CellTrace dilution was assessed 72 hours later. Detection of IL-2 (BD OptEIA, BD Biosciences) was performed by ELISA following the manufacturer's recommendations. In other experiments, BMDCs generated from *Pik3cg$^{-/-}$* or WT animals were pulsed with 25 μg/ml MOG$_{35–55}$ for 6 hours. $5 × 10^4$ DCs were cultured with $10 × 10^4$ CellTrace-labeled 2D2 T cells. Proliferation was assessed 72 hours later.

GeneChip hybridization and data analysis. Total RNA from DCs isolated from spleen and dLNs of tolerized/MOG$_{35–55}$–immunized or MOG$_{35–55}$–immunized mice, 9 days following immunization, was prepared, and hybridization and analysis were performed as described (22). All original microarray data were deposited in the NCBI's Gene Expression Omnibus (GEO GSE47210).

qPCR analysis. DCs were isolated as described above, followed by reverse transcription with ThermoScript Reverse Transcriptase Kit (Invitrogen). Transcripts were quantified by incorporation of Platinum SYBR Green (Bio-Rad Laboratories Inc.) with a Step One Plus Real-Time PCR System (Applied Biosystems), and expression was calculated by the change-in-threshold method ($ΔΔC_T$) with *Hprt* mRNA (encoding hypoxanthine phosphoribosyltransferase 1). For specific primers, see Supplemental Experimental Procedures.

Western blot analysis. Whole-cell lysates (40 μg protein) were subjected to SDS-PAGE electrophoresis on 12% gels and then transferred to Immobilon-P^{sq} membrane (Millipore). For details and Abs, see Supplemental Experimental Procedures.

ChIP assay. $15 × 10^6$ cells were crosslinked with 1% (vol/vol) formaldehyde (followed by extensive wash with PBS) and lysed with lysis buffer. Chromatin was sheared by Covaris Sonicator System to 200- to 400-bp fragments. For more details, see Supplemental Experimental Procedures.

Immunoprecipitation assay. Immunoprecipitation assay is described in Supplemental Experimental Procedures.

RA subjects. Peripheral blood samples were obtained from patients diagnosed with RA according to the 1987 American College of Rheumatology (ACR) criteria (63). At the time of sampling, all patients had residual disease (DAS > 2.8) according to the score based on the 28 joint counts (42). RA patients were treated with anti–TNF-α or CTLA4-Ig (Bristol-Myers Squibb).

Human cell isolation from peripheral blood. Heparinized blood (20 ml) was collected from healthy subjects and RA patients. PBMCs were isolated on Histopaque-1077 (Sigma-Aldrich) density gradient. Briefly, blood was diluted 1:1 with PBS and carefully layered over Histopaque medium. Tubes were centrifuged at 400 *g* for 30 minutes with no break at room temperature. PBMC layer was collected, and cells were washed with PBS.

Human DC generation assay. In order to generate DCs, CD14$^+$ cells were isolated from PBMCs using CD14 microbeads (Miltenyi Biotec). Cells were cultured in the presence of 100 ng/ml IL-4 and 100 ng/ml GM-CSF (Peprotech) for 5 days at $2 × 10^6$ cells/ml in RPMI 1640. At

day 3, 100 ng/ml IL-4 and GMCSF were added. At day 5, cells were collected and treated with 0.5 μg/ml LPS and 100 μg/ml CTLA4-Ig (Bristol-Myers Squibb) in the presence or absence of 20 μM Ly294002 (Cell Signaling) and collected 16 hours later.

Statistics. Statistical analyses were performed using 2-tailed Student's *t* test. Two-way ANOVA statistical tests were applied in experiments with multiple comparisons. Data are presented as mean ± SEM. Differences were considered statistically significant at $P < 0.05$. All data were analyzed using GraphPad Prism v5 software.

Study approval. Patients and healthy individuals were recruited through the Rheumatology and Clinical Immunology Department, Fourth Clinical Pathology, Attikon University Hospital. The Clinical Research Ethics Board of both hospitals (Attikon University Hospital and Hippokration General Hospital, Athens, Greece) approved this study. Informed consent was obtained from all patients and healthy individuals prior to sample collection. For animal studies, all procedures were in accordance with institutional guidelines and were approved by the Greek Federal Veterinary Office.

Author contributions

Acknowledgments

Address correspondence to: Panayotis Verginis, Center of Clinical, Experimental Surgery, and Translational Research, Biomedical Research Foundation, Academy of Athens, 115 27 Athens, Greece. Phone: 30.210.6597516; Email: pverginis@bioacademy.gr.

1. Littman DR, Rudensky AY. Th17 and regulatory T cells in mediating and restraining inflammation. *Cell*. 2010;140(6):845–858.

2. Sakaguchi S, Yamaguchi T, Nomura T, Ono M. Regulatory T cells and immune tolerance. *Cell*. 2008;133(5):775–787.

3. Onishi Y, Fehervari Z, Yamaguchi T, Sakaguchi S. Foxp3+ natural regulatory T cells preferentially form aggregates on dendritic cells in vitro and actively inhibit their maturation. *Proc Natl Acad Sci U S A*. 2008;105(29):10113–10118.

4. Tang Q, et al. Visualizing regulatory T cell control of autoimmune responses in nonobese diabetic mice. *Nat Immunol*. 2006;7(1):83–92.

5. Matheu MP, et al. Imaging regulatory T cell dynamics and CTLA4-mediated suppression of T cell priming. *Nat Commun*. 2015;6:6219.

6. Tadokoro CE, et al. Regulatory T cells inhibit stable contacts between CD4+ T cells and dendritic cells in vivo. *J Exp Med*. 2006;203(3):505–511.

7. Wing K, et al. CTLA-4 control over Foxp3+ regulatory T cell function. *Science*. 2008;322(5899):271–275.

8. Deretic V. Autophagy: an emerging immunological paradigm. *J Immunol*. 2012;189(1):15–20.

9. Qureshi OS, et al. Trans-endocytosis of CD80 and CD86: a molecular basis for the cell-extrinsic function of CTLA-4. *Science*. 2011;332(6029):600–603.

10. Munn DH, Sharma MD, Mellor AL. Ligation of B7-1/B7-2 by human CD4+ T cells triggers indoleamine 2,3-dioxygenase activity in dendritic cells. *J Immunol*. 2004;172(7):4100–4110.

11. Grohmann U, et al. CTLA-4-Ig regulates tryptophan catabolism in vivo. *Nat Immunol*. 2002;3(11):1097–1101.

12. Puccetti P, Grohmann U. IDO and regulatory T cells: a role for reverse signalling and non-canonical NF-κB activation. *Nat Rev Immunol*. 2007;7(10):817–823.

13. Levine B, Deretic V. Unveiling the roles of autophagy in innate and adaptive immunity. *Nat Rev Immunol*. 2007;7(10):767–777.

14. Nedjic J, Aichinger M, Emmerich J, Mizushima N, Klein L. Autophagy in thymic epithelium shapes the T-cell repertoire and is essential for tolerance. *Nature*. 2008;455(7211):396–400.

15. Pua HH, Dzhagalov I, Chuck M, Mizushima N, He YW. A critical role for the autophagy gene Atg5 in T cell survival and proliferation. *J Exp Med*. 2007;204(1):25–31.

16. Espert L, et al. Autophagy is involved in T cell death after binding of HIV-1 envelope proteins to CXCR4. *J Clin Invest*. 2006;116(8):2161–2172.

17. Dengjel J, et al. Autophagy promotes MHC class II presentation of peptides from intracellular source proteins. *Proc Natl Acad Sci U S A*. 2005;102(22):7922–7927.

18. Paludan C, et al. Endogenous MHC class II processing of a viral nuclear antigen after autophagy. *Science*. 2005;307(5709):593–596.

19. Schmid D, Pypaert M, Münz C. Antigen-loading compartments for major histocompatibility complex class II molecules continuously receive input from autophagosomes. *Immunity*. 2007;26(1):79–92.

20. Lee HK, et al. In vivo requirement for Atg5 in antigen presentation by dendritic cells. *Immunity*. 2010;32(2):227–239.

21. Aichinger M, Wu C, Nedjic J, Klein L. Macroautophagy substrates are loaded onto MHC class II of medullary thymic epithelial cells for central tolerance. *J Exp Med*. 2013;210(2):287–300.

22. Alissafi T, et al. De novo-induced self-antigen-specific Foxp3+ regulatory T cells impair the accumulation of inflammatory dendritic cells in draining lymph nodes. *J Immunol*. 2015;194(12):5812–5824.

23. Menssen A, et al. SiPaGene: A new repository for instant online retrieval, sharing and meta-analyses of GeneChip expression data. *BMC Genomics*. 2009;10:98.

24. Fujita N, Itoh T, Omori H, Fukuda M, Noda T, Yoshimori T. The Atg16L complex specifies the site of LC3 lipidation for membrane biogenesis in autophagy. *Mol Biol Cell*. 2008;19(5):2092–2100.

25. Mizushima N, et al. Mouse Apg16L, a novel WD-repeat protein, targets to the autophagic isolation membrane with the Apg12-Apg5 conjugate. *J Cell Sci*. 2003;116(pt 9):1679–1688.

26. Klionsky DJ, et al. Guidelines for the use and interpretation of assays for monitoring autophagy (3rd edition). *Autophagy*. 2016;12(1):1–222.

27. Kabeya Y, et al. LC3, a mammalian homologue of yeast Apg8p, is localized in autophagosome membranes after processing. *EMBO J*. 2000;19(21):5720–5728.

28. Pankiv S, et al. p62/SQSTM1 binds directly to Atg8/LC3 to facilitate degradation of ubiquitinated protein aggregates by autophagy. *J Biol Chem*. 2007;282(33):24131–24145.

29. Ponpuak M, et al. Delivery of cytosolic components by autophagic adaptor protein p62 endows autophagosomes with unique antimicrobial properties. *Immunity*. 2010;32(3):329–341.

30. Martina JA, Chen Y, Gucek M, Puertollano R. MTORC1 functions as a transcriptional regulator of autophagy by preventing nuclear transport of TFEB. *Autophagy*. 2012;8(6):903–914.

31. Ganley IG, Lam du H, Wang J, Ding X, Chen S, Jiang X. ULK1.ATG13.FIP200 complex mediates mTOR signaling and is essential for autophagy. *J Biol Chem*. 2009;284(18):12297–12305.

32. Reggiori F, Komatsu M, Finley K, Simonsen A. Selective types of autophagy. *Int J Cell Biol*. 2012;2012:156272.

33. Hubbard-Lucey VM, et al. Autophagy gene Atg16L1 prevents lethal T cell alloreactivity mediated by dendritic cells. *Immunity*. 2014;41(4):579–591.

34. Petherick KJ, et al. Pharmacological inhibition of ULK1 kinase blocks mammalian target of rapamycin (mTOR)-dependent autophagy. *J Biol Chem*. 2015;290(48):28726.

35. Shevach EM. Mechanisms of Foxp3+ T regulatory cell-mediated suppression. *Immunity*. 2009;30(5):636–645.

36. Klocke K, Sakaguchi S, Holmdahl R, Wing K. Induction of autoimmune disease by deletion of CTLA-4 in mice in adulthood. *Proc Natl Acad Sci U S A*. 2016;113(17):E2383–E2392.

37. Mizushima N, Yoshimori T, Levine B. Methods in mammalian autophagy research. *Cell*. 2010;140(3):313–326.

38. Patrucco E, et al. PI3Kgamma modulates the cardiac response to chronic pressure overload by distinct kinase-dependent and -independent effects. *Cell*. 2004;118(3):375–387.

39. Koorella C, Nair JR, Murray ME, Carlson LM, Watkins SK, Lee KP. Novel regulation of CD80/CD86-induced phosphatidylinositol 3-kinase signaling by NOTCH1 protein in interleukin-6 and indoleamine 2,3-dioxygenase production by dendritic cells. *J Biol Chem*. 2014;289(11):7747–7762.

40. Füllgrabe J, Klionsky DJ, Joseph B. The return of the nucleus: transcriptional and epigenetic control of autophagy. *Nat Rev Mol Cell Biol*. 2014;15(1):65–74.

41. Fiorentino L, et al. Loss of TIMP3 underlies diabetic nephropathy via FoxO1/STAT1 interplay. *EMBO Mol Med*. 2013;5(3):441–455.

42. Prevoo ML, van 't Hof MA, Kuper HH, van Leeuwen MA, van de Putte LB, van Riel PL. Modified disease activity scores that include twenty-eight-joint counts. Development and validation in a prospective longitudinal study of patients with rheumatoid arthritis. *Arthritis Rheum*. 1995;38(1):44–48.

43. Schmid D, Munz C. Innate and adaptive immunity through autophagy. *Immunity*. 2007;27(1):11–21.

44. Bhattacharya A, Parillon X, Zeng S, Han S, Eissa NT. Deficiency of autophagy in dendritic cells protects against experimental autoimmune encephalomyelitis. *J Biol Chem*. 2014;289(38):26525–26532.

45. Kanayama M, Danzaki K, He YW, Shinohara ML. Lung inflammation stalls Th17-cell migration en route to the central nervous system during the development of experimental autoimmune encephalomyelitis. *Int Immunol*. 2016;28(9):463–469.

46. Miyazaki T, et al. Mice lacking H2-M complexes, enigmatic elements of the MHC class II peptide-loading pathway. *Cell*. 1996;84(4):531–541.

47. Martin WD, Hicks GG, Mendiratta SK, Leva HI, Ruley HE, Van Kaer L. H2-M mutant mice are defective in the peptide loading of class II molecules, antigen presentation, and T cell repertoire selection. *Cell*. 1996;84(4):543–550.

48. Slavin AJ, et al. Requirement for endocytic antigen processing and influence of invariant chain and H-2M deficiencies in CNS autoimmunity. *J Clin Invest*. 2001;108(8):1133–1139.

49. Tompkins SM, Padilla J, Dal Canto MC, Ting JP, Van Kaer L, Miller SD. De novo central nervous system processing of myelin antigen is required for the initiation of experimental autoimmune encephalomyelitis. *J Immunol*. 2002;168(8):4173–4183.

50. Roche PA, Furuta K. The ins and outs of MHC class II-mediated antigen processing and presentation. *Nat Rev Immunol*. 2015;15(4):203–216.

51. Liu H, et al. Ubiquitin ligase MARCH 8 cooperates with CD83 to control surface MHC II expression in thymic epithelium and CD4 T cell selection. *J Exp Med*. 2016;213(9):1695–1703.

52. Patakas A, et al. Abatacept inhibits T cell priming by inducing of a unique transcriptional profile that reduces their ability to activate antigen presenting cells. *Arthritis Rheumatol*. 2016;68(3):627–638.

53. Codogno P, Mehrpour M, Proikas-Cezanne T. Canonical and non-canonical autophagy: variations on a common theme of self-eating? *Nat Rev Mol Cell Biol*. 2011;13(1):7–12.

54. Carman JA, et al. Abatacept does not induce direct

gene expression changes in antigen-presenting cells. *J Clin Immunol*. 2009;29(4):479–489.

55. Zhou J, et al. FOXO3 induces FOXO1-dependent autophagy by activating the AKT1 signaling pathway. *Autophagy*. 2012;8(12):1712–1723.

56. Sengupta A, Molkentin JD, Yutzey KE. FoxO transcription factors promote autophagy in cardiomyocytes. *J Biol Chem*. 2009;284(41):28319–28331.

57. Dejean AS, et al. Transcription factor Foxo3 controls the magnitude of T cell immune responses by modulating the function of dendritic cells. *Nat Immunol*. 2009;10(5):504–513.

58. Fallarino F, et al. CTLA-4-Ig activates forkhead transcription factors and protects dendritic cells from oxidative stress in nonobese diabetic mice. *J Exp Med*. 2004;200(8):1051–1062.

59. Nakae J, Park BC, Accili D. Insulin stimulates phosphorylation of the forkhead transcription factor FKHR on serine 253 through a Wortmannin-sensitive pathway. *J Biol Chem*. 1999;274(23):15982–15985.

60. Wang S, et al. FoxO1-mediated autophagy is required for NK cell development and innate immunity. *Nat Commun*. 2016;7:11023.

61. Ioannou M, et al. Crucial role of granulocytic myeloid-derived suppressor cells in the regulation of central nervous system autoimmune disease. *J Immunol*. 2012;188(3):1136–1146.

62. Lutz MB, et al. An advanced culture method for generating large quantities of highly pure dendritic cells from mouse bone marrow. *J Immunol Methods*. 1999;223(1):77–92.

63. Arnett FC, et al. The American Rheumatism Association 1987 revised criteria for the classification of rheumatoid arthritis. *Arthritis Rheum*. 1988;31(3):315–324.